UNIVERSIDADE DA BEIRA INTERIOR
Engenharia

Roll Motion Control of a Dissymmetrical Wingspan Aircraft

Filipe Miguel Tanqueiro Tavares

Dissertação para obtenção do Grau de Mestre em
Engenharia Aeronáutica
(2º ciclo de estudos)

Orientador: Professor Kouamana Bousson
Co-orientador: Professor Pedro Gamboa

Covilhã, Outubro de 2011

Acknowledgements

Firstly, I would like to gratefully thank all my family, which, with great difficulties, never ceased to provide everything I needed for the duration of my stay here in Covilhã. Without them, I would not even be writing this work.

Secondly, I have to thank my supervisors, Kouamana Bousson and Pedro Gamboa, for the help and enlightenment provided along the course, without which not even a third of the studies presented here would have been made possible for me.

Thirdly, my greatest thank and love goes to my girlfriend Stephanny, which was able to understand my dedication and forgive all the time spent away doing this.

Lastly, a big *thank you* goes to all my friends who were able to show support and friendship along the last six years. Without you all, I may not have been able to find the forces to finish this work.

Abstract

The present study focuses on the design of a controller for an unmanned aircraft using a variable-span dissymmetric system. This is primarily intended to stabilize roll, although it was designed as a robust system for total control. The system in use is new in its application, being studied similar aircraft built to date. The aircraft for which the system has been designed is an experimental UAV built entirely at the University of Beira Interior. The stability derivatives and other data were obtained with the help of XFLR software. The development and simulation were done using MATLAB, where were tested two different control methods, LQR and Batz-Kleinman controller. A review of the flight dynamics equations for a standard aircraft was originally done, being then adapted this new concept. The interaction between the control surfaces and the response of a general aircraft was studied. An implementation of predetermined flying qualities in order to scale the state weight matrix in the LQR controller for optimal levels was also performed. At the end three separate simulations were performed to confirm the validity of the theoretical system in control and stabilization, for leveled flight when suffering disturbances, and for various equilibrium states described by a sinusoidal equation and a random variation.

Keywords

Dissymmetric wing, variable span, UAV, robust controller, roll control, LQR, Batz-Kleinman controller.

Resumo

O presente estudo concentra-se no projecto de um controlador para uma aeronave não tripulada usando um sistema de asa de envergadura dissimétrica e variável. Este visa primeiramente estabilizar o rolamento, embora tenha sido projectado um sistema robusto de controlo total. O sistema em uso é pioneiro na sua aplicação, tendo sido estudadas semelhantes aeronaves construídas até à data. A aeronave para qual o sistema foi dimensionado é um UAV experimental construído totalmente na Universidade da Beira Interior. As derivadas de estabilidade e restantes dados aerodinâmicos foram obtidos com a ajuda do software XFLR. O desenvolvimento e simulação foram realizados em software MATLAB, para o qual são testados dois métodos de controlo distintos, com LQR e controlador Batz-Kleinman. Foi inicialmente feita uma revisão das equações da dinâmica de voo para uma aeronave generalizada, sendo depois adaptado o novo conceito em estudo. A interacção entre as superfícies de controlo gerais e a resposta de uma aeronave foi estudada. Uma implementação de qualidades de voo pré-determinadas com vista a dimensionar a matriz de pesos de estado no controlador LQR para níveis óptimos foi também realizada. No final foram feitas três simulações distintas para confirmar teoricamente a validade do sistema no controlo e estabilização, em voo nivelado sofrendo perturbações, e consoante pontos de equilíbrio pré-determinados segundo uma equação sinusoidal e para uma variação aleatória.

Palavras-chave

Asa dissimétrica, envergadura variável, UAV, controlador robusto, controlo do rolamento, LQR, controlador Batz-Kleinman.

Index

Chapter 1 1

Introduction 1

1.1 Control Surfaces 2

1.1.1 Global Flight Dynamics 3

1.1.2 Longitudinal Flight 7

1.1.3 Lateral-Directional Flight 9

1.2 Stability Derivatives 12

1.3 Flight Modes (Handling Qualities) 13

1.3.1 Longitudinal Flight Modes 14

1.3.2 Lateral Flight Modes 14

1.4 Control with Classical Surfaces 15

1.4.1 LQR Controller 16

1.4.2 Batz-Kleinman Controller 18

1.5 Block Diagram of a Control System 19

Chapter 2 21

Variable-Span Aircraft 21

2.1 Dissymmetrical Span Interest 23

2.2 Dissymmetrical Span Control 24

Chapter 3 31

Simulation and Tests 31

3.1 Imposed Flying Qualities 31

3.2 Classical Control Method (Disturbance Response) 33

3.3 Bank Angle Sinusoidal Variation 39

3.4 Random Bank Angle Variation (Two Step Maximum) 44

Chapter 4 47

Conclusions 47

Bibliography 49

Appendix i

A - UAV “Olharapo” drawings i

B - Handling Qualities Data iii

C - Paper vii

List of Figures

Figure 1.1 *Wright Brothers* flying machine (1903) [1] 1
Figure 1.2 *Blériot XI* (above) and *Levavasseur Antoinette IV* (below) sketches [2].....2
Figure 1.3 Diagrammatic sketch of a simple airplane control system [2] 3
Figure 1.4 Schematic diagram of stick-elevator linkage [3].....3
Figure 1.5 a) Earth and body (aircraft) axis system [4]; b) Forces, moments, angles and angular velocities acting on an aircraft [4] 4
Figure 1.6 Control surfaces and positive deflections in general [4] 4
Figure 1.7 Forces and angles in longitudinal flight [3] 7
Figure 1.8 Relation between the angle of attack (α) and angle of path (γ) in perturbed flight [4] 7
Figure 1.9 Pressure distribution along the tail and change due to elevator deflection [3] 9
Figure 1.10 Effect on angle of attack due to elevator deflection [3] 9
Figure 1.11 Forces and moments present on a levelled flight aircraft [3] 9
Figure 1.12 Aircraft orientation on the horizontal plane [3]..... 10
Figure 1.13 Sideslip angle (β) corrected by a rudder deflection (δr) [3] 11
Figure 1.14 Relationship between the yaw (ψ) and sideslip (β) angles [3]..... 11
Figure 1.15 Aileron deflection and signal convention [3]..... 12
Figure 1.16 Development of sideslip due to bank [3] 12
Figure 1.17 Control system scheme [13]..... 15
Figure 1.18 General block diagram of an AFCS [4]..... 19
Figure 1.19 Closed loop state regulator with optimal feedback [4] 20
Figure 2.1 Variable sweep (left); Telescopic wing (centre); Extendable wing (right) [18]..... 21
Figure 2.2 *Ivan Makhonine's MAK-123* [19]..... 22
Figure 2.3 The *Akaflieg FS-29* sailplane [20]..... 22
Figure 2.4 Genesis different configurations [21]..... 23
Figure 2.5 Variable-Span Wing mechanical system (1-servo-motor; 2- transmission pinion; 3-transmission rack; 4-carbon spar) [24]..... 24
Figure 2.6 Theory for aileron effectiveness approximation [7]..... 25
Figure 2.7 Roll moment coefficient (Cl) distribution due to wing deflection (y)..... 26
Figure 2.8 Yaw moment coefficient (Cn) distribution due to wing deflection (y)..... 27
Figure 2.9 Wing deflection variable for: a) Flight with wings extended, below 20 m/s; b) Flight with wings retracted, above 20 m/s..... 28
Figure 2.10 Span variation with flight speed (left) and drag reduction relative to original wing (right) for the original and variable-span wings [23]. 29
Figure 3.1 Short-period parameters from pilot opinions [6] 32
Figure 3.2 Diagram of program simulation flow scheme (in general) 34

Figure 3.3 Classic disturbance simulation response with LQR for x1 36
Figure 3.4 Classic disturbance simulation response with Batz-Kleinman for x1 37
Figure 3.5 Detailed roll control and state variables for classic simulation with LQR (left) and Batz-Kleinman (right) 37
Figure 3.6 Classic disturbance simulation response with LQR for x2 38
Figure 3.7 Classic disturbance simulation response with Batz-Kleinman for x2 39
Figure 3.8 Sinusoidal variation of the bank angle (maximum bank 30 degrees, time 120 seconds, for y1) 40
Figure 3.9 LQR simulation for a sinusoidal variation of bank for y1 41
Figure 3.10 Batz-Kleinman simulation for a sinusoidal variation of bank for y1 41
Figure 3.11 Detailed roll control and state variables for sinusoidal simulation with LQR (left) and Batz-Kleinman (right) for y1 42
Figure 3.12 LQR simulation for a sinusoidal variation of bank for y2 43
Figure 3.13 Batz-Kleinman simulation for a sinusoidal variation of bank for y2 43
Figure 3.14 Detailed roll control and state variables for sinusoidal simulation with LQR (left) and Batz-Kleinman (right) for y2 44
Figure 3.15 Random bank simulation using LQR for z1 45
Figure 3.16 Detailed roll control and state variables for random simulation with LQR for z1. 45
Figure 3.17 Detailed roll control and state variables for random simulation with LQR for z2. 46

List of Tables

Table 2.1 Zero angle of attack coefficients..... 27
Table 2.2 Longitudinal stability and control derivatives..... 27
Table 2.3 Lateral-directional stability and control derivatives..... 28
Table 2.4 Aircraft and flight conditions data 29
Table 2.5 Inertial moments assumed..... 29
Table 3.1 Level 1, Class I, Cat. B corresponding parameters for each flight mode..... 32
Table 3.2 Variables chosen for Eigen value calculation..... 33
Table 3.3 Equilibrium State constants 34
Table 3.4 Equilibrium Control constants..... 34

Nomenclature

α	Angle of Attack
β	Sideslip Angle
θ	Pitch Angle
ϕ	Bank Angle
ψ	Yaw Angle
γ	Path Angle
δ_e	Elevator Deflection
δ_a	Aileron Deflection
δ_r	Rudder Deflection
p	Roll Rate
q	Pitch Rate
r	Yaw Rate
m	Mass
V	Aircraft Speed
t	Time
C	Kinetic Moment
L	Roll Moment
M	Pitch Moment
N	Yaw Moment
u	Longitudinal Speed
v	Lateral Speed
w	Vertical Speed
C_L	Lift Coefficient
C_{L_0}	Lift Coefficient for a Zero Angle of Attack
C_{L_α}	Lift Coefficient for a given Angle of Attack
$\bar{c}$	Median Chord
C_{L_q}	Lift Coefficient due to Pitch Rate
$C_{L_{\delta_e}}$	Lift Coefficient due to Elevator Deflection
C_D	Drag Coefficient
C_{D_0}	Drag Coefficient for a Zero Angle of Attack
K_{C_D}	Drag Coefficient Factor
C_{D_α}	Drag Coefficient for a given Angle of Attack
C_{D_q}	Drag Coefficient due to Pitch Rate
C_y	Lateral Force Coefficient
C_{y_β}	Lateral Force Coefficient due to Sideslip Angle
$C_{y_{\delta_a}}$	Lateral Force Coefficient due to Aileron Deflection
$C_{y_{\delta_r}}$	Lateral Force Coefficient due to Rudder Deflection

C_l	Roll Moment Coefficient
C_{l_β}	Roll Moment Coefficient due to Sideslip Angle
b	Span
C_{l_p}	Roll Moment Coefficient due to Roll Rate
C_{l_r}	Roll Moment Coefficient due to Yaw Rate
$C_{l_{\delta_a}}$	Roll Moment Coefficient due to Aileron Deflection
$C_{l_{\delta_r}}$	Roll Moment Coefficient due to Rudder Deflection
C_m	Pitch Moment Coefficient
C_{m_0}	Pitch Moment Coefficient for a Zero Angle of Attack
C_{m_α}	Pitch Moment Coefficient for a given Angle of Attack
C_{m_q}	Pitch Moment Coefficient due to Pitch Rate
$C_{m_{\delta_e}}$	Pitch Moment Coefficient due to Elevator Deflection
C_n	Yaw Moment Coefficient
C_{n_β}	Yaw Moment Coefficient due to Sideslip Angle
C_{n_p}	Yaw Moment Coefficient due to Roll Rate
C_{n_r}	Yaw Moment Coefficient due to Yaw Rate
$C_{n_{\delta_a}}$	Yaw Moment Coefficient due to Aileron Deflection
$C_{n_{\delta_r}}$	Yaw Moment Coefficient due to Rudder Deflection
I_{xx}	Inertial Moment about the Longitudinal axis
I_{yy}	Inertial Moment about the Lateral axis
I_{zz}	Inertial Moment about the Vertical axis
I_{xz}	Inertial Moment with respect to the xz-plane
Q	Dynamic Pressure
S	Wing Area
ρ	Air Density
T	Thrust
g	Gravity Acceleration
δ_T	Throttle Setting
h	Altitude
C_T	Thrust Coefficient
$C_{T\delta_T}$	Thrust Coefficient due to Throttle Setting
δ_y	Wing Span Variation
δ_{V_e}	V-Tail Elevator Deflection Component
δ_{V_r}	V-Tail Rudder Deflection Component
$C.G.$	Centre of Gravity
AFS	Akademische Fliegergruppe Stuttgart
LQR	Linear Quadratic Regulator
AFCS	Automatic Flight Control System
λ	Eigenvalue
ξ	Damping Ratio
ω_n	Natural Frequency

Chapter 1

Introduction

Nowadays people tend to look at the sky and see a passing airplane and do not consider the work that is behind it. Building and flying an airplane can be achieved by almost anyone with a basic knowledge of the dynamics of flight, but most simply may not foresee the consequences of a badly designed rudder or a very small dihedral on the main wings. All these mistakes lay on the concepts of stability and control, i.e., a stable airplane is often very easy to control. The optimization of most aspects surrounding an aircraft dynamics requires some mean calculations, and is subject to the various conditions during a flight, i.e., take-off, climbing turn, levelled cruise, approach, landing. For each optimal adjustment of the aircraft control surfaces, span and wing aspect would be preferred as it minimises the energy losses during flight. Fortunately today airplane enthusiasts are developing a long observed but not easy to build concept: *morphing*. By altering the shape of the wing, for example, the drag forces can be minimized, which allows for a faster flight with the same energy loss. Birds have been doing it since they started flying, and the first men who flew did it without really understanding the benefits it would bring.

When *Orville* and *Wilbur Wright* took the important step in aviation in 1903 [1], they were the first to recognize the crucial importance of airplane stability. Only after the experience of first flight, the need for a light and powerful engine, the stability aspect, and the means to create some sort of control was given true importance in flying, besides the fact that a pilot is crucial to maintain this stability through small corrective changes in attitude.

Figure 1.1 *Wright Brothers* flying machine (1903) [1]

The *Wright Brothers* pioneered these first acknowledgements. Along with the remarkable achievement, they were the first to recognize that, for example: an airplane had to be banked to turn in a horizontal plane; a linked interaction exists between the banking (or roll control) and the yawing motion of an airplane; excessive dihedral effects hinder pilot control

unless sideslip is suppressed and makes the machine unduly sensitive to atmospheric turbulence; wings can be stalled, leading to loss in control; and control can be regained after stalling by reducing the angle of attack [1] [2]. Even with their achievements they had built a very unstable and difficult to fly aircraft, and between 1904 and 1905, they did improve lateral stability by removing the negative dihedral angle on the wings (as seen in Figure 1.1), reduced longitudinal instability by ballasting it to be more nose-heavy, and improved its lateral control by removing the mechanical roll–yaw control interconnect.

Two public demonstrations of perfectly controlled mechanical flight in 1908 by *Wilbur Wright*, in France, and by *Orville Wright* in the United States were wakeup calls to the rest of the aeronautical community who run to catch up with and surpass the *Brother's* achievements, and by 1910, the biggest airplane makers at the time had built machines (Figure 1.2) that flew faster and almost as well. By 1911 they flew better.

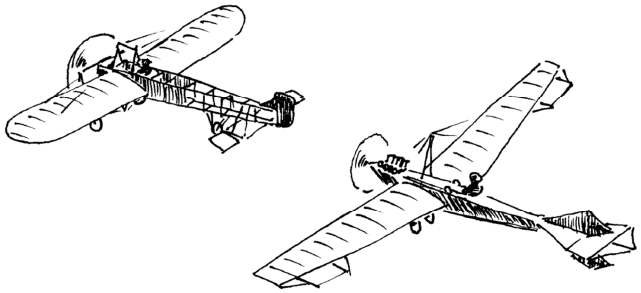

Figure 1.2 *Blériot XI* (above) and *Levavasseur Antoinette IV* (below) sketches [2]

However, even after these momentous achievements, neither the Wrights nor their competitors still had any real understanding of aerodynamic theory, and things were achieved mostly by trial and error.

1.1 Control Surfaces

Before flap-type control surfaces tabs had been invented, roll control was achieved by wrapping the wing (seen nowadays as wing *morphing*). It was in 1908 that the aviation pioneer *Glenn Curtiss* made the first flight of his *June Bug* airplane, which was equipped with flap-type lateral controls. These control surface tabs are small movable surfaces at the trailing edge, or rear, of a wing's aerofoil. Tabs generate aerodynamic pressures that operate with a long moment arm about the control surface hinge line. They provide an effective way to deflect the main control surfaces in a direction opposite to the force it creates. This concept was introduced by *Anton Flettner* who first applied it to steamboat rudders.

By 1917, after trial and error building during the First World War, it became established that the optimal configuration and control methods for a somehow stable aircraft was the shown

in Figure 1.3. It was *Louis Blériot* who introduced the standards of the control system with a central control stick linked to the ailerons and elevator, and a handlebar linked to the rudder.

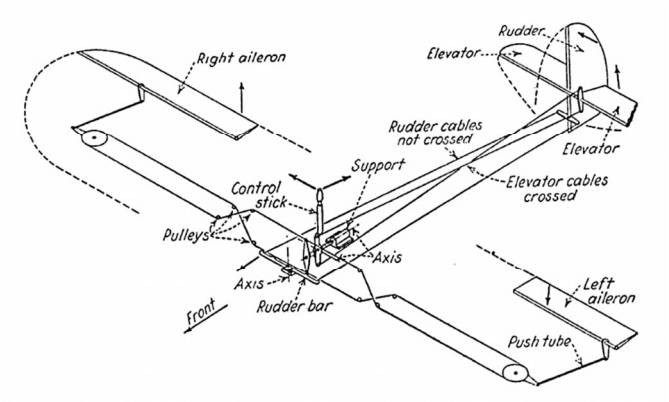

Figure 1.3 Diagrammatic sketch of a simple airplane control system [2]

Blériot's rudder system, now quite standard, is controlled by moving the handlebar in the opposite way of bicycle turning. All the other connections and wiring is standardly crossed to allow the correct motion response to the corresponding control stick input (Figure 1.4).

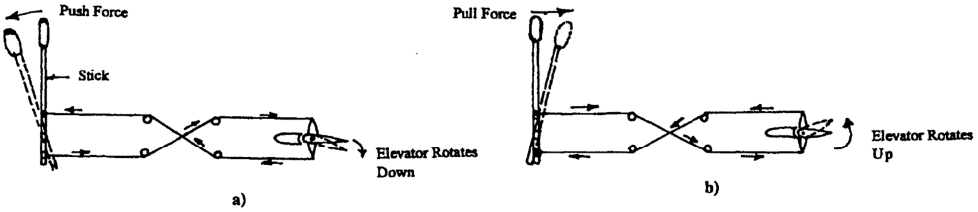

Figure 1.4 Schematic diagram of stick-elevator linkage [3]

Nowadays, the standard control system follows this one introduced with the first flying craft. Resuming, generally it is distributed by the wings and tail, which have movable hinged tabs to change the normal aerodynamic pressure distribution in order to generate a resultant force on the wing or tail stabilizer. Of course this only works if we have air moving through the wing's control surface, and the faster it moves, considering a zero angle of attack on the wing or stabilizer, the bigger the pressure varies with the angle of the control surface.

1.1.1 Global Flight Dynamics

The dynamic analysis of an airplane is made with no consideration of any elastic forces such as wing torsion, so it is seen as a rigid-body object with an associated axis system. Generally one fixed and centred on the aircraft centre of gravity ($\mathcal{R}_b = (\vec{x}, \vec{y}, \vec{z})$), and another fixed to earth ($\mathcal{R}_0 = (\vec{x}_0, \vec{y}_0, \vec{z}_0)$) as in Figure 1.5 a) [3] [4] [5]. On a flying airplane act aerodynamic, traction and gravitational forces, being these plus the angles and variation rates relative to the corresponding axis represented in Figure 1.5 b).

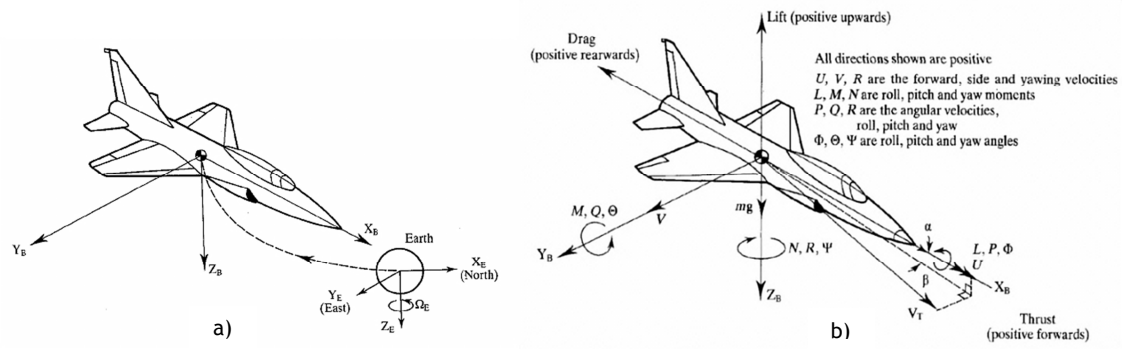

Figure 1.5 a) Earth and body (aircraft) axis system [4]; b) Forces, moments, angles and angular velocities acting on an aircraft [4]

All moments are positive in the directions also shown in Figure 1.5 b), which later define the orientation of the airplane motion. Considering V_T as the aerodynamic speed reference for the aircraft, we obtain the angles of attack (α), sideslip (β), pitch (θ), bank (ϕ) and yaw (ψ), being the last three (θ, ϕ and ψ) the manoeuvring angles related to the corresponding axis which define the attitude of the airplane. These are *Euler* angles [3] [4] [5] [6], and represent the three rotations in order to the relative axis. The attitude angles are directly influenced by the control surfaces as expected. For example, by deflecting the elevator (δe) the pitch angle (θ) suffers a change. The same is valid for the rest of the control deflections (δr and ψ; δa and ϕ). To maintain these manoeuvring angles constant, for a stable aircraft, it is necessary to deflect the corresponding control surfaces up to a given angle, i.e. *trimming*.

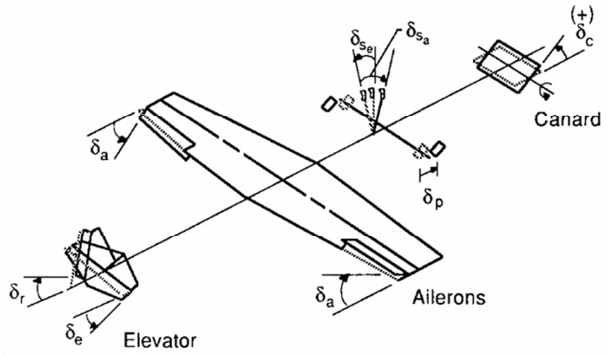

Figure 1.6 Control surfaces and positive deflections in general [4]

The time-derivatives of the *Euler* attitude angles may be computed from the attitude rates (p, q and r), which represent the "quantity of motion" about the respective axis. These are the basics that describe an airplane attitude and motion rate. To better understand the laws that manage the full dynamics of flight, it becomes necessary to formulate the equations for the force and moment coefficients.

A flying aircraft represents a very complicated dynamic system. To determine the flight dynamic equations which relate all the last attitude variables, it is necessary to review *Newton's* second law (1.1 and 1.2) [5]:

$$m\frac{dV}{dt} = \sum_i \vec{F}_i \quad (1.1)$$

$$\frac{dC}{dt} = \sum_i M_i \quad (1.2)$$

Where, $\sum_i \vec{F}_i$ is the sum of all external forces and $\sum_i M_i$ is the sum of all the moments associated with the external forces, all actuating on the airplane.

From the *Euler* angles seen in Figure 1.5 b) and the velocity components (u, v, w) we can write the general equations that describe the airplane $C.G.$ (centre of gravity) position along the Earth reference axis [3] [5] [6] [7]:

$$\dot{x} = u\cos\psi\cos\theta + v(\cos\psi\sin\theta\sin\phi - \sin\psi\cos\phi) + w(\sin\psi\sin\phi + \cos\psi\sin\theta\cos\phi) \quad (1.3)$$

$$\dot{y} = u\sin\psi\cos\theta + v(\cos\psi\cos\phi + \sin\psi\sin\theta\sin\phi) + w(\sin\psi\sin\theta\cos\phi - \cos\psi\sin\phi) \quad (1.4)$$

$$\dot{h} = u\sin\theta - v\cos\theta\sin\phi - w\cos\theta\cos\phi \quad (1.5)$$

Where $\dot{h}$ is equivalent to $-\dot{z}$.

By measuring the angular variation of each attitude angle, we can obtain the angular velocities:

$$p = \dot{\phi} - \dot{\psi}\sin\theta \quad (1.6)$$

$$q = \dot{\theta}\cos\phi + \dot{\psi}\cos\theta\sin\phi \quad (1.7)$$

$$r = \dot{\psi}\cos\theta\cos\phi - \dot{\theta}\sin\phi \quad (1.8)$$

The cinematic equations for the attitude angles (or attitude rates), deducted from the attitude angles and angular velocities (p, q, r) are:

$$\dot{\phi} = p + (q\sin\phi + r\cos\phi)\tan\theta \quad (1.9)$$

$$\dot{\theta} = q\cos\phi - r\sin\phi \quad (1.10)$$

$$\dot{\psi} = \frac{q\sin\phi + r\cos\phi}{\cos\theta} \quad (1.11)$$

This defines the position and angle rates of an airplane. Before determining the complete flight equations it is necessary to define the aerodynamic coefficients. These are composed by small incremental variations of the dimensionless coefficients [8] (stability derivatives) multiplied by the corresponding variables, which depend on the aircraft and flight conditions:

Generally, lift (C_L), drag (C_D) and lateral force (C_y) coefficients are defined by:

$$C_L = C_{L_0} + C_{L_\alpha}\alpha + \frac{\bar{c}}{2V}\left(C_{L_{\dot{\alpha}}}\dot{\alpha} + C_{L_q}q\right) + C_{L_{\delta_e}}\delta_e \quad (1.12)$$

$$C_D = C_{D_0} + K_{C_D}C_L^2 \text{ or } C_D = C_{D_0} + C_{D_\alpha}\alpha + \frac{\bar{c}}{2V}\left(C_{D_{\dot{\alpha}}}\dot{\alpha} + C_{D_q}q\right) + C_{L_{\delta_e}}\delta_e \quad (1.13)$$

$$C_y = C_{y_\beta}\beta + C_{y_{\delta_a}}\delta_a + C_{y_{\delta_r}}\delta_r \quad (1.14)$$

Note that C_{D_0} and K_{C_D} are constants for the used aerofoil.

And roll (C_l), pitch (C_m) and yaw (C_n) coefficients by:

$$C_l = C_{l_\beta}\beta + \frac{b}{2V}\left(C_{l_p}p + C_{l_r}r\right) + C_{l_{\delta_a}}\delta_a + C_{l_{\delta_r}}\delta_r \quad (1.15)$$

$$C_m = C_{m_0} + C_{m_\alpha}\alpha + \frac{\bar{c}}{2V}\left(C_{m_{\dot{\alpha}}}\dot{\alpha} + C_{m_q}q\right) + C_{m_{\delta_e}}\delta_e \quad (1.16)$$

$$C_n = C_{n_\beta}\beta + \frac{b}{2V}\left(C_{n_p}p + C_{n_r}r\right) + C_{n_{\delta_a}}\delta_a + C_{n_{\delta_r}}\delta_r \quad (1.17)$$

With $\dot{\alpha} = \frac{u\dot{w} - \dot{u}w}{u^2 + w^2}$. (1.18)

With this we can now write the velocity equations [5]:

$$\dot{u} = -\frac{QS}{m}\left(C_D\cos\alpha\cos\beta + C_y\cos\alpha\sin\beta - C_L\sin\alpha\right) + \frac{T}{m} - g\sin\theta - qw + rv \quad (1.19)$$

$$\dot{v} = -\frac{QS}{m}\left(C_D\sin\beta - C_y\cos\beta\right) + g\cos\theta\sin\phi - ru + pw \quad (1.20)$$

$$\dot{w} = -\frac{QS}{m}\left(C_D\sin\alpha\cos\beta + C_y\sin\alpha\sin\beta + C_L\cos\alpha\right) + g\cos\theta\cos\phi - pv + qu \quad (1.21)$$

With $T = \delta_T T_{max}(V, h)$, for a given speed and altitude. (1.22)

The equations for the manoeuvring taxes are mainly determined from the inertia of the airplane:

$$\dot{p} = \frac{1}{I_{xx}I_{yy} - I_{xz}^2}\left[I_{zz}\left(QSbC_l + \left(I_{yy} - I_{zz}\right)qr\right) + I_{xz}\left(QSbC_n + \left(I_{xx} - I_{yy} + I_{zz}\right)pq - I_{xz}qr\right)\right] \quad (1.23)$$

$$\dot{q} = \frac{1}{I_{yy}}[QScC_m + I_{xz}(r^2 - p^2) + (I_{zz} - I_{xx})rp] \quad (1.24)$$

$$\dot{r} = \frac{1}{I_{xx}I_{yy} - I_{xz}^2}\left[I_{xx}\left(QSbC_n + \left(I_{xx} - I_{yy}\right)pq\right) + I_{xz}\left(QSbC_l + \left(I_{yy} - I_{xx} - I_{zz}\right)qr + I_{xz}pq\right)\right] \quad (1.25)$$

Where the dynamic pressure is $Q = 0.5\rho V^2$. (1.26)

To fully comprehend the relationship between the control surface deflections and the effect on the attitude angles, it is convenient to analyse separately the behaviour of the airplane in longitudinal flight and then in lateral-directional flight.

1.1.2 Longitudinal Flight

Simplifying the flight equations only for the longitudinal plane by considering null the effects of all non-longitudinal parameters and thus locking the velocity vector, we obtain the modified equations necessary to fully describe an airplane motion along this plane. For this matter, the control variables are also reduced to the elevator deflection (δ_e) and throttle variation (δ_T), and the airplane describes only climbing/descending motions. For unperturbed flight, the pitch (θ) and path (γ) angles are equal as seen in Figure 1.7:

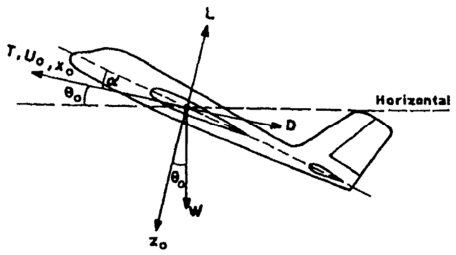

Figure 1.7 Forces and angles in longitudinal flight [3]

For longitudinal flight, sideslip (β), roll (ϕ) and yaw (ψ) angles are considered null:

$$\beta = 0 \;;\; \phi = 0 \;;\; \psi = 0 \quad (1.27)$$

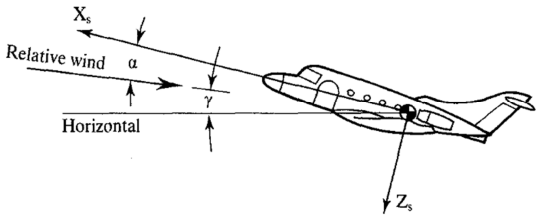

Figure 1.8 Relation between the angle of attack (α) and angle of path (γ) in perturbed flight [4]

The path angle formed between the velocity vector and the horizontal plane (or in this case the horizontal axis) is related to the attack and pitch angles as [4] [5]:

$$\theta = \alpha + \gamma \tag{1.28}$$

And the attack angle relates to the longitudinal and vertical velocities as [5]:

$$u = V\cos\alpha \tag{1.29}$$

$$w = V\sin\alpha \tag{1.30}$$

$$\alpha = \operatorname{atan}\frac{w}{u} \tag{1.31}$$

Simplifying with these relations and null parameters, the only applied coefficients are:

$$C_D = C_{D0} + C_{D\alpha}\alpha + C_{D\delta_e}|\delta_e| \tag{1.32}$$

$$C_L = C_{L0} + C_{L\alpha}\alpha + C_{L\delta_e}\delta_e + C_{Lq}\frac{q\bar{c}}{2V} + C_{L\dot{\alpha}}\frac{\dot{\alpha}\bar{c}}{2V} \tag{1.33}$$

$$C_m = C_{m_0} + C_{m\alpha}\alpha + C_{m\delta_e}\delta_e + C_{mq}\frac{q\bar{c}}{2V} + C_{m\dot{\alpha}}\frac{\dot{\alpha}\bar{c}}{2V} \tag{1.34}$$

Also, the necessary flight equations reduce to:

$$\dot{u} = \frac{1}{m}(0.5\rho(h)Su^2(1+\tan^2\alpha)(C_L\sin\alpha - C_D\cos\alpha) + T\cos\varepsilon_T) - g\sin\theta - qw \tag{1.35}$$

$$\dot{w} = \frac{1}{m}\left(T\sin\varepsilon_T - 0.5\rho(h)Su^2(1+\tan^2\alpha)(C_D\sin\alpha - C_L\cos\alpha)\right) + g\cos\theta + qu \tag{1.36}$$

$$\dot{q} = \frac{\rho(h)u^2(1+\tan^2\alpha)S\bar{c}C_m}{2I_{yy}} \tag{1.37}$$

$$\dot{\theta} = q \tag{1.38}$$

With $T = \frac{1}{2}\rho(h)Su^2(1+\tan^2\alpha)C_T$ and $C_T = C_{T\delta_T}\delta_T$. (1.39)

Here the interest lies on the resulting angle of attack (α) (and therefore pitch and path angles from 1.28) given a deflection of the elevator (δ_e). The system works by changing the pressure distribution around the horizontal tail, which (normally) has a symmetric profile, and so altering the pitch moment (M) (Figure 1.9). From the flight equations we can then obtain the

resulting angle of attack, pitch angle and pitch rate (α, θ, and q). For a positive deflection of δ_e results a negative angle of attack α as shown in Figure 1.10.

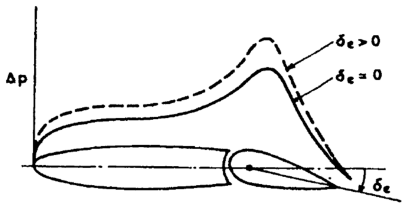

Figure 1.9 Pressure distribution along the tail and change due to elevator deflection [3]

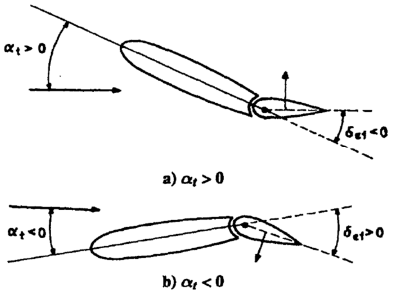

Figure 1.10 Effect on angle of attack due to elevator deflection [3]

This change in pitch moment is also acknowledged by the deviation in lift forces on the tail's empennage as it differs from the levelled lift (Figure 1.11).

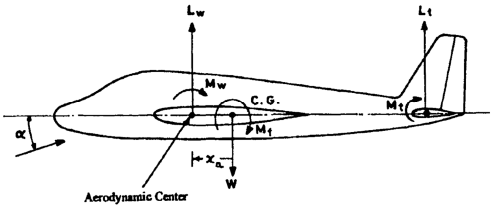

Figure 1.11 Forces and moments present on a levelled flight aircraft [3]

The variation of thrust (δ_T) by the throttle also influences the attitude of the airplane, as it tends to increase speed adding more lift, and consequently increasing also the angle of attack, making it necessary to compensate with the elevator to maintain levelled flight.

1.1.3 Lateral-Directional Flight

In this analysis, now only looking at the motion described on the lateral and directional planes, the previous variables do not apply. For directional flight we consider only the lateral velocity (v), the yaw angle (ψ) and the yaw rate (r); for lateral flight only the bank angle (ϕ) and the roll rate (p). Both motions are interlinked. This is noticed when an airplane makes a controlled turn which induces roll and yaw variations simultaneously, and therefore a deflection of the *ailerons* (δ_a) and rudder (δ_r) respectively.

For this flight mode, similarly to the previous motion, the only applied moment coefficients are [5]:

$$C_D = C_{D0} + C_{D\alpha}\alpha + C_{D\delta_e}|\delta_e| \quad (1.40)$$

$$C_y = C_{y_\beta}\beta + C_{y_{\delta_a}}\delta_a + C_{y_{\delta_r}}\delta_r \quad (1.41)$$

$$C_l = C_{l_\beta}\beta + \frac{b}{2V}\left(C_{l_p}p + C_{l_r}r\right) + C_{l_{\delta_a}}\delta_a + C_{l_{\delta_r}}\delta_r \quad (1.42)$$

$$C_n = C_{n_\beta}\beta + \frac{b}{2V}\left(C_{n_p}p + C_{n_r}r\right) + C_{n_{\delta_a}}\delta_a + C_{n_{\delta_r}}\delta_r \quad (1.43)$$

The pitch angle (θ) and therefore the angle of attack (α) are considered null and the general flight equations are then reduced to [5]:

$$\dot{v} = -\frac{QS}{m}\left(C_D\sin\beta - C_y\cos\beta\right) + g\cos\theta_0\sin\phi - ru_0 + pw_0 \quad (1.44)$$

Where β is given from (1.49). (1.45)

$$\dot{p} = \frac{1}{I_{xx}I_{yy} - I_{xz}^2}\left(I_{zz}\left(QSbC_l + \left(I_{yy} - I_{zz}\right)qr\right) + I_{xz}\left(QSbC_n + \left(I_{xx} - I_{yy} + I_{zz}\right)pq - I_{xz}qr\right)\right) \quad (1.46)$$

$$\dot{r} = \frac{1}{I_{xx}I_{yy} - I_{xz}^2}\left(I_{xx}\left(QSbC_n + \left(I_{xx} - I_{yy}\right)pq\right) + I_{xz}\left(QSbC_l + \left(I_{yy} - I_{xx} - I_{zz}\right)qr - I_{xz}pq\right)\right) \quad (1.47)$$

$$\dot{\phi} = p + r\cos\phi\tan\theta_0 \quad (1.48)$$

Considering the horizontal plane, the sideslip angle (β) is obtained from a lateral disturbance (Figure 1.12), i.e., a change in wind direction.

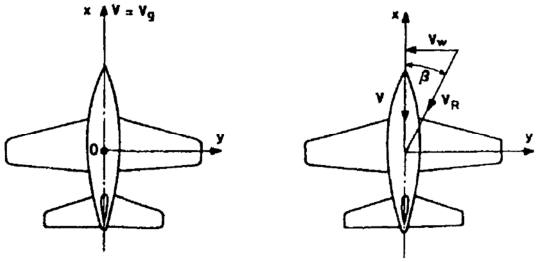

Figure 1.12 Aircraft orientation on the horizontal plane [3]

The sideslip angle is related to the airplane velocities from Figure 1.12 [3] [5]:

$$\beta = \operatorname{asin}\frac{v}{V} \quad (1.49)$$

A sideslip angle (β) is corrected by a rudder deflection (δ_r) (Figure 1.13) in order to maintain the desired flight path. The rudder works the same way as the elevator by changing the pressure gradient around the tail, but here we usually have only one vertical wing located above the gravity's centre ($C.G.$) horizontal plane, which also induces a small roll moment on the airplane.

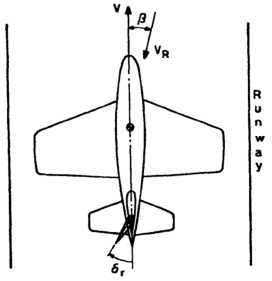

Figure 1.13 Sideslip angle (β) corrected by a rudder deflection (δ_r) [3]

In the special case when the airplane velocity (V) matches the same direction as the flight path, i.e., approaching with a lateral wind at constant and relative speed (Figure 1.13), the yaw angle (ψ) can be related to the sideslip angle (β) by:

$$\psi = -\beta \tag{1.50}$$

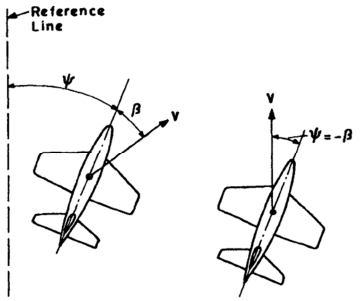

Figure 1.14 Relationship between the yaw (ψ) and sideslip (β) angles [3]

This angle (ψ) is also seen as the bearing of the airplane. As it is an angle which does not depend on any aerodynamic forces or moments (usually associated to the sideslip angle (β) correction), it normally is not considered in the flight equations and does not enter on control purposes [3] [5].

Analysing now the motion around the vertical plane, we have the bank angle (ϕ), which is obtained from the pressure gradient between the left and right wings, due to a symmetric deflection of the ailerons (δ_a). This symmetric deflection changes the roll moment around the longitudinal axis (C_l) as shown in Figure 1.15.

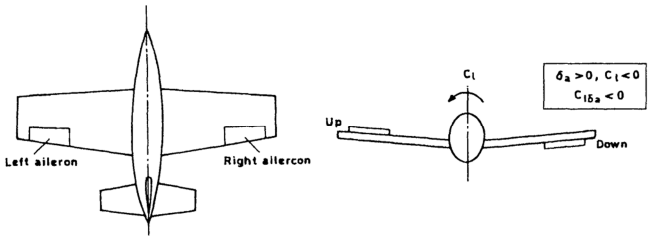

Figure 1.15 Aileron deflection and signal convention [3]

With this angle of bank, the aircraft tends to develop a sideslip as shown in Figure 1.16, which can be corrected with a deflection of the rudder (δ_r). This way it is comprehensive the need for a linked operation between the ailerons and rudder control surfaces, in order to perform a levelled turn.

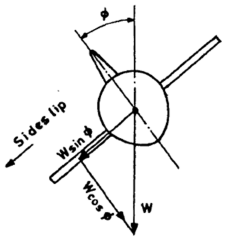

Figure 1.16 Development of sideslip due to bank [3]

An effect of the deflection of the ailerons is the inducing of yaw (also known as adverse yaw [7]) where the airplane yaws its nose due to the asymmetry of drag from the *ailerons* (the one deflected down has more induced drag than the other one). This has to be corrected by the pilot or control mechanism to avoid entering a spin for instance.

1.2 Stability Derivatives

The stability derivatives describe the change to a force or moment in response to a variation of a flight variable. In order to fully and precisely determine the influences of the various angles and rates to the moment and force coefficients, it becomes favourable to analyse the airplane in-flight. As this is not viable in project phase, these have to be estimated using several equations available throughout several books [3] [6] [7]. This estimation is based on known flight equations and relations between variables and moments.

Fortunately today we have software available [9] that, using the equations mentioned before, actually perform a thorough analysis and delivers all the needed derivatives and inertial moments with a fairly accurate precision. This software was indeed used later to simulate the actual forces and moments in flight, and estimate the stability coefficients, which proved to be very precise and somewhat easy to use.

1.3 Flight Modes (Handling Qualities)

A trimmed airplane performs a natural frequency motion when disturbed from equilibrium. In order to understand the principles behind this theory, we must first understand the concept of stability, which divides into static and dynamic stabilities. An airplane is in equilibrium when the resultant forces and moments about the $C.G.$ are equal to zero, and the tendency for an airplane to return to this equilibrium, after a disturbance, is the concept of static stability. For this to happen, the airplane must have restoring moments or forces. In dynamic stability we focus on what happens to the motion of the airplane, when suffering a disturbance, through time. Here we can have two options: oscillatory (damped or undamped) and non-oscillatory motions [4] [7]. One important thing to notice is that an airplane can be statically stable but dynamically unstable, but if it is dynamically stable than it must be statically stable as well.

This theory was first developed by *George H. Bryan* in 1904 [10], and he developed it before knowing about Wright brother's first flight. He showed that there are several longitudinal and lateral flying modes which can be oscillatory or not. The ability to control an airplane due to these flight modes defines the handling qualities of the vehicle.

The oscillatory modes can be described by a second-order equation, based on the principle of a rigid body coupled to a spring and a damping device [7]. The spring has a natural frequency of ω_n and the damping device a damping ratio of ξ. As such, this system has a characteristic equation in the following form:

$$\lambda^2 + 2\xi\omega_n\lambda + {\omega_n}^2 = 0 \qquad (1.51)$$

Where the two roots, in the form $\lambda = a \pm bi$, are given by:

$$\lambda_{1,2} = -\xi\omega_n \pm i\omega_n\sqrt{1-\xi^2} \qquad (1.52)$$

In the 60's, to better understand and classify the quality of an airplane behaviour, a unique evaluation system was developed called the *Cooper-Harper scale* [5] [6] [7]. Three flying levels where created (Levels 1, 2 and 3), four airplane classes (Class I, II, III and IV), and three flight phase categories (Cat. A, B and C). These are described with precision on various books and on the web [5] [6] [7] [11], and are presently annexed. According to these flight levels, classes and categories, there are certain limits to the natural frequency, damping ratio and period for each mode that define the respective flying characteristics of the airplane. Each mode's respective Eigen value is obtained from the characteristic equation of

the state matrix A. It is important to notice that negative eigenvalues refer to converging motions, which represent dynamically stable flying modes.

1.3.1 Longitudinal Flight Modes

In longitudinal flight two modes can be acknowledged: phugoid (long-period) and short-period oscillations. The phugoid motion is created when, locking the angle of attack, there is a natural oscillatory motion with variations of speed, altitude and attitude. This flight mode is dependant only of the equilibrium speed of a given airplane. This can be acknowledged when flying a paper plane or a glider above or below the best gliding speed.

The short-period oscillation consists of a rotation around the yy axis of the vehicle when affected by a vertical disturbance. During this mode the speed is constant and the attitude angles deviate from equilibrium. As the name suggests, the short-period has a shorter oscillation period than the phugoid. This allows the identification of each conjugated eigenvalue, where the period is determined by:

$$T_p = \frac{2\pi}{\omega_n\sqrt{1-\xi^2}} \tag{1.53}$$

The real and imaginary parts for each eigenvalue are determined by equation 1.52.

1.3.2 Lateral Flight Modes

In lateral flight three modes of motion are present: spiral, roll and Dutch roll (being the last the only oscillatory, very similar to short-period). The spiral motion is the tendency to increase or reduce the wing bank angle after a lateral disturbance [5]. The vehicle performs a turn, with the turn radius affected by its stability characteristics. As it is not an oscillatory mode, the corresponding eigenvalue is obtained from a logarithmic function, and the only limiting data is the minimum time to double its amplitude, given by:

$$T_2 = \frac{\log(2)}{-\lambda} \tag{1.54}$$

The spiral mode eigenvalue is the smallest real absolute value of all four.

The Dutch roll motion resembles a “falling leaf” type oscillation which consists of a combination of yaw and roll motion. The conjugated eigenvalue is determined similarly to the phugoid, and is easy to identify.

The roll mode, as the spiral mode, is not oscillatory and depends on the bank angle. The only variable that characterizes this eigenvalue is the total roll time and is calculated with:

$$T_t = \frac{1}{-\lambda} \quad (1.55)$$

This is the biggest real absolute value of all four.

1.4 Control with Classical Surfaces

History has shown over time that if stability and control are neglected when designing an aircraft, accidents tend to happen. Every aspiring airplane maker sees the need for an adequate engine and rigid structures, but many omit the proper positioning of the gravity centre ($C.G.$) or optimal dimensioning of the control surface areas to allow for the most effective manoeuvrability, i.e., recovering from a spin. The amount of energy required to operate a poorly designed airplane is also a negative factor, and minimizing this energy loss is the main characteristic of an optimal control system.

Up to now we have seen how is the dynamics of an airplane influenced by the deflection of control surfaces and a disturbance of the flight conditions, both in longitudinal and lateral-directional flight modes. As seen, in case of a small disturbance of the equilibrium flight conditions we define, most airplanes are not sufficiently stable to return to this previous state [3]. As described on Chapter 1, this was first realised by earlier flights, where a pilot was the most important asset in an airplane to maintain its stability [1] [2]. Nowadays systems have evolved and an automatic controller can effectively maintain the attitude of an airplane by means of an actuator and electrical motor (Figure 1.17), enabling the pilot to concentrate more on other aspects of flight and allowing some aircraft to even fly, such as the *F-117 "Nighthawk"* [12].

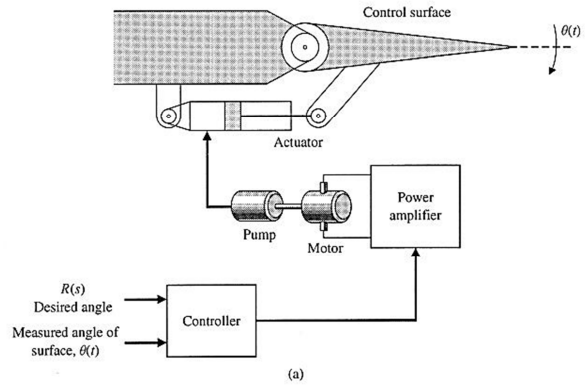

Figure 1.17 Control system scheme [13]

The development of an automatic control system (or autopilot) started early [14]. About 1914, the *Sperry Brothers* proved it was indeed possible to maintain the attitude of an airplane in flight, if the airplane was dynamically stable, even suffering several random disturbances.

Nowadays there are several methods to stabilize the attitude variables of an aircraft. The most commonly used is the PID controller (proportional–integral–derivative controller) [15], which calculates an error value as the difference between a measured process variable and a desired objective point, and then attempts to minimize this error by adjusting the process control inputs. A better alternative to this method is the use of a LQR controller.

1.4.1 LQR Controller

LQR stands for *Linear Quadratic Regulator*. Implementing a LQR controller implies operating a dynamic system at minimum cost with supplied weight factors (R and Q matrices). This system dynamics must be described by a set of linear differential equations, which, in the case of the non-linear flight equations explained on Chapter 1 (equations 1.35-1.39;1.44-1.48), these have to be linearized. To do so, the equilibrium state must also be defined in order to linearize the system around it, and to apply the LQR control. The most common equilibrium state is levelled (trimmed) flight.

As such, a continuous-time linear system is described by (1.56) [2] [3] [4] [5] [6]:

$$\begin{cases} \dot{x} = Ax + Bu \\ y = Cx + Du \end{cases} \tag{1.56}$$

The cost function is defined as (1.57):

$$J = \int_0^\infty F(x, u)\, dt \tag{1.57}$$

Where:

$$F(x, u) = x^T Q x + u^T R u \tag{1.58}$$

Q and R are weighting matrixes for state and control variables, respectively, and must be positive-definite (being Q positive semi-definite).

The feedback control law that minimizes the cost equation in (1.57) is:

$$u = -Kx \tag{1.59}$$

K is the system's gain matrix with m lines and n columns ($K \in \mathbb{R}^{m\,x\,n}$) and is determined by (1.60):

$$K = R^{-1}B^{T}P \tag{1.60}$$

P is found by solving the continuous time algebraic Riccati [5] equation in (1.61):

$$A^{T}P + PA - PBR^{-1}B^{T}P + Q = 0 \tag{1.61}$$

The cost function J (1.57) is often defined as a sum of the deviations of key measurements from their desired values. In effect this algorithm therefore finds those controller settings that minimize the undesired deviations, like deviations from the desired attitude.

The main problem with properly (optimally) scaling a LQR controller is finding the adequate weighting factors R and Q, and this somehow limits the utilization of this controller. R and Q can be simply determined using *Bryson's* method [5], where each state and control weight is calculated in relation to its maximum amplitude:

$$Q_{ii} = {}^{1}\!/_{x_{i,max}^{2}} \qquad R_{ii} = {}^{1}\!/_{u_{i,max}^{2}} \tag{1.62}$$

This method lacks the proper optimization aspects as it is somehow limited for state values, which maximum values are not easily determined. Control limits are given by the maximum physical properties of the control surfaces. This method is a good starting point for trial-and-error iterations searching for the desired controller results.

Jia Luo and C. Edward Lan [16] purposed another method for this estimation. The R matrix is still determined using *Bryson's* method [5] (1.62) and the problem lies in the determination of an optimal Q. For this it is necessary to first minimize the cost function J (1.57) by use of the *Hamiltonian* matrix (H) which is used to determine (P) in LQR. This matrix (H) is defined as:

$$H \in \mathbb{R}^{2n\times 2n} \equiv \begin{bmatrix} A & -BR^{-1}B^{T} \\ -Q & -A^{T} \end{bmatrix} \tag{1.63}$$

The eigenvalues of this matrix are symmetrically distributed along the imaginary axis, thus having positive and negative symmetric real parts. To determine those eigenvalues, the following algebraic equation needs to be solved:

$$\det(\lambda_{i}I - H) = 0 \tag{1.64}$$

With this equation (1.64) we can also determine the matrix Q, but for this the eigenvalues (λ_i) need to be assumed, which gives us some power for optimization. For simple calculations it is enough to use the eigenvalues of the state matrix A, but if we want to minimize the cost function J (1.57) imposing certain flight qualities, these eigenvalues are then subject to our needs. The weighting matrix Q is defined by one single diagonal composed with a vector $q_i = (q_1, q_2, \dots, q_n)$. The problem is finding the q_i that satisfies (1.64), and one can do that by minimizing the following equation system:

$$f_i(q_i) = \det(\lambda_i I - H(q_i)) = 0 \quad (1.65)$$

Being:

$$Q_{ii} = q_i \quad (1.66)$$

As Q is positive semi-definite, in case of any of the diagonal values found with solving (1.65) being negative, we can simply elevate them to square. Another way is to use the absolute value of any negative element. This enables us to find the right R and Q.

The control law to apply in the controller as the feedback system is given by (1.59). The system stabilizes around zero with this equation. To force a convergence to a given equilibrium state and control points (x_{ref}, u_{ref}), these points are included in the control law as:

$$u = u_{ref} - K(x - x_{ref}) \quad (1.67)$$

With this the system fully stabilizes an aircraft state and control variables to the equilibrium values, in order to some optimization of the R and Q weighting matrixes.

1.4.2 Batz-Kleinman Controller

This method is very similar to the LQR method, except the gain matrix K (1.60) is here seen as an L matrix, as it is defined by (1.68) [17]:

$$L = B^T * P(\tau)^T \quad (1.68)$$

Where P is now defined by the *Gramian* as (1.69) [17]:

$$P(\tau) = \int_0^{\tau} e^{-A*t} * B * B^T * e^{-A^T*t} dt \quad (1.69)$$

A variable τ appears here to limit the integration interval and is assumed (always positive) for optimization purposes. The smaller the variable τ, the smaller the control amplitude, and the faster it converges for optimal values.

The control law here is the same as LQR but with the L matrix defined in (1.68):

$$u = u_{ref} - L(x - x_{ref}) \quad (1.70)$$

Several other control methods exist [5] [17], being these the most effective ones.

1.5 Block Diagram of a Control System

When designing a complete state regulator for an airplane, the full system block diagram becomes crucial to understand and to further build it physically. This scheme is composed by all the sub-systems that influence the flight variables, either being motion sensors or controlling elements. Generally, an AFCS (*Automatic Flight Control System*) is represented as shown in Figure 1.18. For specific motion regulators (i.e., lateral motion, specific state variables) a simplified system is designed but based on the same general idea.

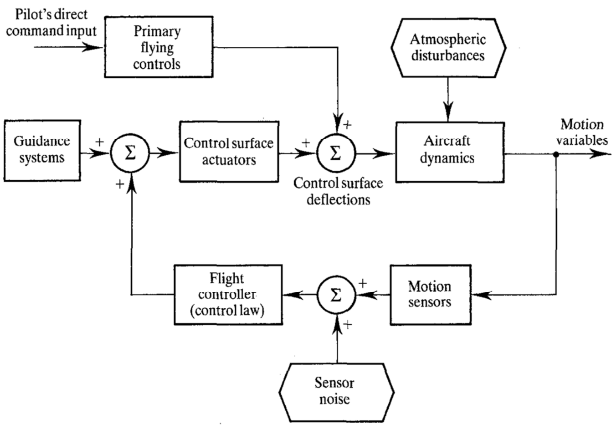

Figure 1.18 General block diagram of an AFCS [4]

By analysing the LQR control method described along this chapter, and structuring it to a block diagram such as the last, a state regulator is usually composed as shown in Figure 1.19. The state and control matrices, composed by the derivatives of the airplane [7], are shown in blocks A and B, and the gain matrix K is the feedback system that minimizes the cost function in 1.57. The input control variables in u are previously determined when linearizing the system for a given equilibrium state, which are iterated to stabilise the state variables in x.

The integral block represents the solution of the system's differential equation $\dot{x} = Ax + Bu$ by means of the control law $u = u_{ref} - K(x - x_{ref})$. The output variable x is the optimized state vector that fulfils the LQR method of control.

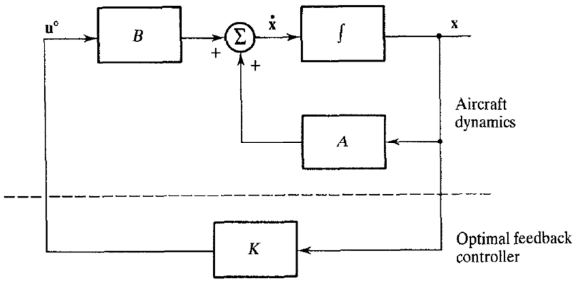

Figure 1.19 Closed loop state regulator with optimal feedback [4]

Chapter 2

Variable-Span Aircraft

The purpose of this work is the implementation of a variable-span system. A variable-span aircraft is able to change span length (b) during flight according to the specified flight conditions. Most airplanes that have a variable-span system use it mainly to reduce drag and optimize flight according to certain requirements. There are several ways to vary the geometry of the wing as seen in Figure 2.1.

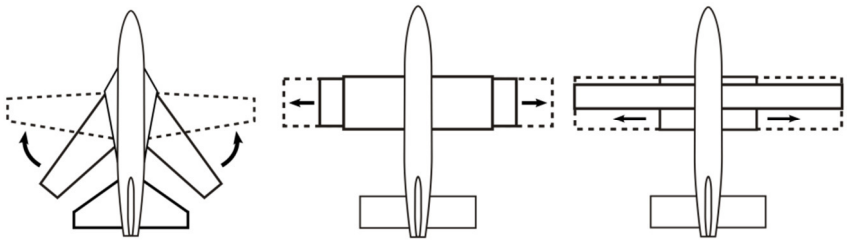

Figure 2.1 Variable sweep (left); Telescopic wing (centre); Extendable wing (right) [18]

The first example seen is the most commonly used where wings sweep back and forth. With both wings unfolded the airplane gains extra overall wingspan, which allows for a slower flight speed and better control on approach/landing/take-off conditions by reducing its stall speed. Both wings retracted permit better manoeuvrability, high cruise speed, and a decrease in wing induced drag. The *F-14 "Tomcat"* is one of the most famous examples of a variable sweep airplane (Figure 2.1 (left)) [12]. Besides this there are several other examples such as: *Tu-160*, *B-1* or *F-111*, and most carrier operational aircraft [12].

The system used in this work is of another kind: variable-span telescopic wing (Figure 2.1 (centre)). It resembles the last but there is no change in sweep angle. Throughout history, the first example of flying variable-span airplane dates 1931 in France when a Russian expatriate, *Ivan Makhonine* first conceived this idea by building and flying the *MAK-10* [19]. The aircraft had a pneumatically powered sliding mechanism to extend and retract both wings symmetrically, which worked well but was severely underpowered. After the war around 1947, *Makhonine's* work continued and he built the *MAK-123* [19] – a four seat aircraft (Figure 2.2). Once again the concept worked well, with the extension system powered by a quarter horse powered motor.

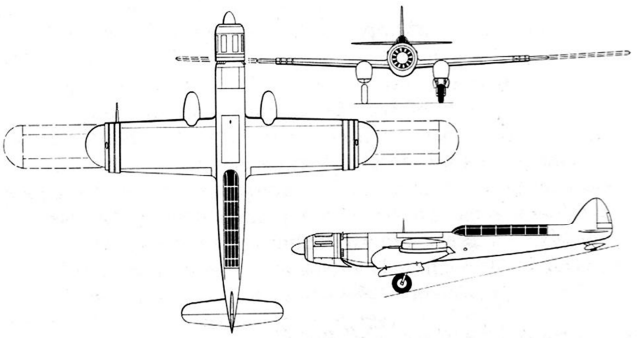

Figure 2.2 *Ivan Makhonine's MAK-123* [19]

Unfortunately the airplane crashed into a potato field when the engine failed during a flight, and the concept became forgotten.

Later in 1975, the *Akademische Fliegergruppe Stuttgart* (*AFS*) designed and built the first and only manned variable-span sailplane up to now, the *Akaflieg FS-29* [20] as seen in Figure 2.3.

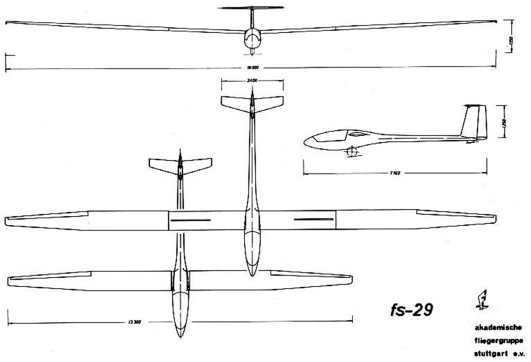

Figure 2.3 The *Akaflieg FS-29* sailplane [20]

With the same concept of telescopic wing, the airplane was able to achieve good soaring/slow speed with the wings extended, and increase its flight range and cruise speed by retracting both wings. The difference was the lack of an engine to power the extension system, so it had to be done manually by the pilot, which proved to be a tedious and distracting job.

Today most work is done theoretically, but some is relevant in this concept. Recently (in 1997) *Gevers Aircraft Inc.* developed the *Genesis* airplane [21], which is not only capable of changing its shape in order to land on different terrain or water surfaces, but also has a telescopic variable-span system allowing to perform very well in flight. Unfortunately there is no evidence of it leaving the paper.

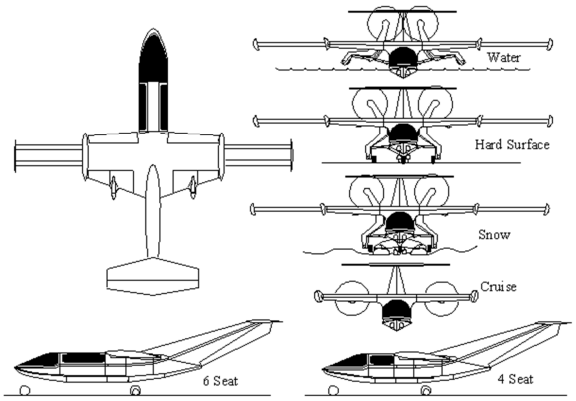

Figure 2.4 Genesis different configurations [21]

More recently (in 2004) *David A. Neal et al.* from *Virginia University* [22] designed, built and tested (in wind tunnel) a fully adaptive wing configuration system, which is able to change span (telescopically) and sweep simultaneously or for the best performance optimization, as well as increase or decrease wing tip twist. The tail also extends making it a 7 degrees of freedom (*DOF*) aircraft.

All the above airplanes and designs are for a symmetrical change of span and sweep. When looking at the concept, the idea of using this span variation asymmetrically to induce a rolling moment the same way ailerons do comes to mind. Unfortunately through time there is not much evidence of those who have tried to design and build airplanes with dissymmetrical-variable-span systems, mostly because of its complexity and weight, but mainly due to the efficiency in control.

2.1 Dissymmetrical Span Interest

In the system studied in this project, left and right wings are fully autonomous, and allow the control of the rolling moment by creating an asymmetry in lift distribution. With this, in theory, we can substitute the *aileron* concept completely, but to become a valid control system, it must allow better or at least the same manoeuvrability as ailerons do. Drag reduction in roll for a dissymmetrical span wing, when comparing it to *ailerons*, is one big advantage [21].

When designing a variable-span airplane, the two mechanisms (aileron and variable-span) are difficult to co-exist. As it is theoretically possible to control the roll moment of a system like this, it makes a very interesting work to develop. When analysing the details behind the two mechanisms, ailerons change the pressure distribution (and with it the lift) along the section of wing where they are built, but a dissymmetrical span wing alters the total pressure curve along the span of the wing. This is a much complex system indeed. Full aileron angle deflection is a lot easier and cheaper (energy cost) to perform when compared to a full (and

equivalent) retraction of one wing section, and it is also lighter to build. That was the main issue of *Makhonine* [19] and *AFS* [20] aircraft as the displacement of the moving wing required a lot of energy and was very influenced by wing load at the time. Time to fully deflect a wing is also a large problem, as for big disturbances of levelled flight conditions the plane must have the necessary authority to return to that state as fast as it can (without compromising its structure).

2.2 Dissymmetrical Span Control

The main goal of this system is to fully control all flight variables of the UAV "Olharapo" (images annexed) with the implementation of a dissymmetric variable-span concept wing. The controller is designed to stabilize every state and control variable to the predefined flight condition, i.e. equilibrium state. The deflection variable for dissymmetric span variation, which substitutes aileron deflection, is now referred as δ_y, where a new approach must be implemented [23]. The dissymmetrical wing system consists of two fully retractable and autonomous wing sections, each moved by a servo and rack mechanism. In Figure 2.5 the final mechanical system can be observed. All design and construction was developed over the last two years by two other aeronautic students.

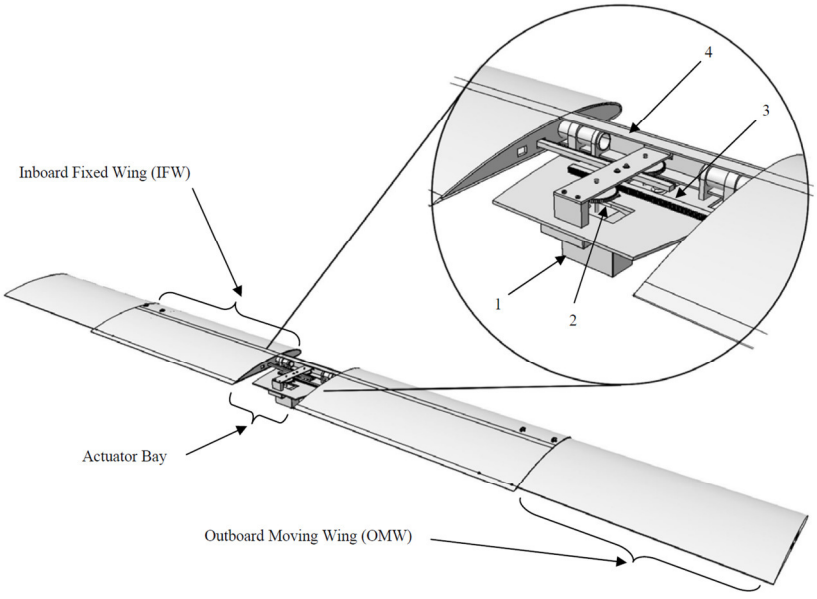

Figure 2.5 Variable-Span Wing mechanical system (1-servo-motor; 2- transmission pinion; 3-transmission rack; 4-carbon spar) [24]

The system must provide roll authority equivalent to the authority provided by the use of ailerons, which means that, for one of the wings, the variation in roll moment coefficient with the deflection of the control surface (or flap) is given by [5] [7]:

$$C_{l_{\delta_a}} = \frac{dC_l}{d\delta_a} = \frac{2C_{l_\alpha}\tau}{Sb}\int_{y_1}^{y_2} cy\, dy \qquad (2.1)$$

Where, τ here refers to the flap effectiveness parameter [7], and y_1, y_2 are the limits of the control surface as in Figure 2.6.

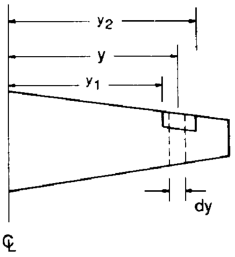

Figure 2.6 Theory for aileron effectiveness approximation [7]

Gamboa et al. [23] demonstrated that, for a symmetric variable span morphing wing and assuming the wing's lift distribution to be perfectly elliptical, moving the elliptic centre along the y-axis, it is possible to obtain $C_{l_{\delta_y}}$ the following way:

$$C_{l_{\delta_y}} = \frac{8W}{\pi b \rho V^2 S_{ref} b_{ref}} \int_{-b'}^{b''} y \sqrt{1 - \left(\frac{2(y - y')}{b}\right)^2}\, dy \tag{2.2}$$

Where, b' and b'' refer to the left and right span dimensions, respectively; y is the length of a semi-wing, and y' is the span deflection. b_{ref} is the wing's maximum span which differs from $b = b' + b''$. This was a valuable starting point as not many other similar researches were found. As this system, similarly to the aileron system, moves the aerodynamic lift distribution centre opposite to the deflected (or retracted wing), the distance from the C.G. creates a moment that forces the airplane to roll.

One other derivative takes a direct part in roll motion and was analysed in this work as well. The damping-in-roll, or C_{l_p}, is the influence of the roll rate p on the roll moment coefficient C_l, also seen as the tendency for an airplane to roll. From the same analysis made for estimating $C_{l_{\delta_y}}$, the damping-in-roll derivative can be estimated as:

$$C_{l_p} = -\frac{1}{V S_{ref} b_{ref}} \int_{-b'}^{b''} a_{0_y}(y) \sqrt{1 - \left(\frac{2(y - y')}{b}\right)^2}\, c(y) y^2 dy \tag{2.3}$$

The roll, yaw and lateral force coefficient equations where the new derivatives take part were modified by simple substitution. This was studied as the equations are composed by incrementing each influential dynamic variable multiplied by its derivative. As such, and with the help of XFLR5 v6.03 software [9], the work was simplified a lot. In theory, by testing the airplane without one of the semi-wings (meaning the full deflection on one side) one should be able to obtain the resulting pressure/lift distribution, and with this, determine the

variation of the roll moment with the deflection of the span. The analysis is then made according to the resultant differential lift (ΔL) below [7]:

$$\Delta C_l = \frac{\Delta L}{QS_{ref}b_{ref}} = \frac{C_L c(y)dy}{S_{ref}b_{ref}} \tag{2.4}$$

By obtaining the lift coefficient (C_L) distribution from XFLR, iterating for various positions of the deflected wing, the resulting variation of the roll moment coefficient (C_l) due to a deflection of the right wing, and symmetrically for the left side, can be seen in Figure 2.7:

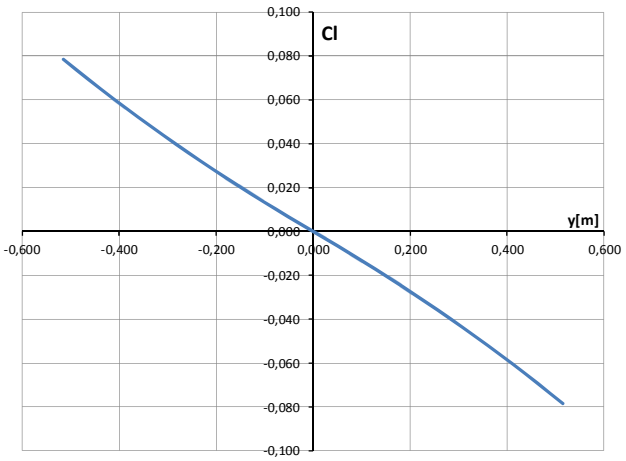

Figure 2.7 Roll moment coefficient (C_l) distribution due to wing deflection (y)

A positive deflection of a wing results in a negative variation of roll moment, as the lift increases on the deflected side.

The influence in yaw moment by *aileron* deflection can be ignored as the control surfaces are reversely linked, i.e., the increase in drag is assumed equal for the left and right *ailerons*. For design and control purposes this means an inconsideration of adverse yaw [7]. As the variable span system works by deflecting only one wing at a time, the variation of drag is not symmetric, and as such, must be considered. A positive deflection (Figure 2.9) of one wing span implies a positive yaw moment increase. To determine an approximate yaw moment variation due to the variation in span, a similar approach as to roll moment (Figure 2.7) was made taking in consideration the total drag coefficient distribution from XFLR analysis, influenced by the parasite and induced drag coefficients ($C_{D,0}, C_{D,i}$). The resulting yaw moment variation was estimated by equation 2.5, and represented in Figure 2.8:

$$\Delta C_n = \frac{\Delta D}{QS_{ref}b_{ref}} = \frac{(C_{D,0} + C_{D,i})c(y)dy}{S_{ref}b_{ref}} \tag{2.5}$$

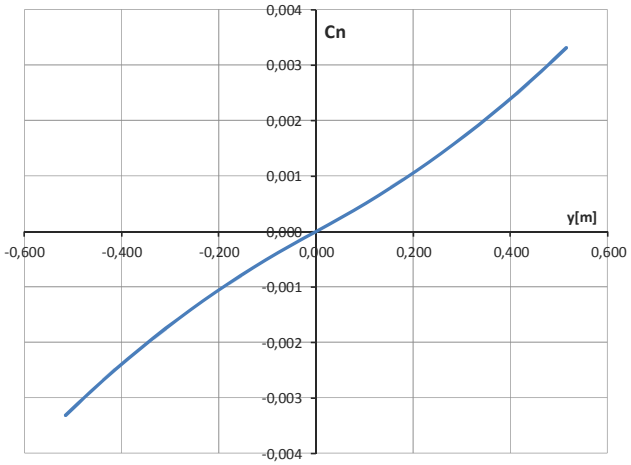

Figure 2.8 Yaw moment coefficient (C_n) distribution due to wing deflection (y)

From the two distributions in Figure 2.7 and Figure 2.8, the control derivatives for $C_{l\delta y}$ and $C_{n\delta y}$ can be obtained. The results are present in Table 2.3 below. The remaining derivative that measures the relation between the wing deflection and the lateral force, $C_{y\delta y}$, can be ignored as laterally it does not influence in a measurable amount. The C_{l_p} and C_{n_r} derivatives, which are affected by induced roll and yaw due to the V-Tail, were assumed from the data obtained in XFLR simulations [6].

All other derivatives were estimated using XFLR. Weight, traction and dimensions were obtained from direct measurements on the airplane. As the UAV is V-Tailed, the respective deflection components for elevator and rudder are replaced as δ_{V_e} and δ_{V_r}, respectively. Other derivatives which refer to these control variables are accordingly written as well. The relations between a V-Tail and a Standard Tail elevator and rudder deflections are found using simple trigonometry functions. As the software used to calculate the stability derivatives (XFLR) already analysis the aerodynamics with the V-Tail built in the model, the resulting elevator and rudder stability derivatives are given considering the relationship between both tail types due to the option to simulate independent control surfaces for each side of the V-Tail.

Running the simulation for a zero angle of attack, the following coefficients were obtained:

Table 2.1 Zero angle of attack coefficients

C_{L0} = 0.19664	C_{D0} = 0.01652	C_{m0} = 0.03526

The final stability and control derivatives for longitudinal flight are:

Table 2.2 Longitudinal stability and control derivatives

$C_{L\alpha}$ = 4.41816	$C_{D\alpha}$ = 0.17321	$C_{m\alpha}$ = -1.44014	C_{Lq} = 7.57384

C_{mq} = -10.28831	$C_{L\delta Ve}$ = 0.71433	$C_{D\delta Ve}$ = 0.036361	$C_{m\delta Ve}$ = -1.8844

The final stability and control derivatives for lateral-directional flight are:

Table 2.3 Lateral-directional stability and control derivatives

$C_{y\beta}$ = -0.17991	$C_{l\beta}$ = -0.04508	$C_{n\beta}$ = 0.05733	C_{lp} = -0.55989
C_{np} = -0.05572	C_{lr} = 0.14868	C_{nr} = -0.03924	$C_{l\delta y}$ = 0.1467
$C_{n\delta y}$ = -0.006	$C_{y\delta Vr}$ = 0.040083	$C_{l\delta Vr}$ = -0.054716	$C_{n\delta Vr}$ = -0.021383

The following derivatives were assumed null as only a very small influence is expected from those:

$$C_{L\dot{\alpha}},\ C_{m\dot{\alpha}},\ C_{y\delta y} = 0 \tag{2.6}$$

To control, one main consideration to take is the dimension of the wing deflection. By taking measurements in the already built airplane "Olharapo", it was noticed that the wing span varies between 1470 millimetres for both wings retracted, and 2500 millimetres for both wings fully extended. This means that each movable wing extends about 515 millimetres, and the wing is able to alter its span by almost double. To apply this in the control, some notions had to be developed. The δ_y control variable is limited by -0.515 to +0.515 metres so that it resembles the working method of all other control variables. This does not represent reality, but a simple way to solve this problem. Flying with both wings extended (or both wings retracted) refers to a null δ_y. With this notion, the wing deflection is related to the actual working scheme as showed in Figure 2.9. Note that the controller is dimensioned for a cruise speed of 20 metres per second, which stands about half its projected speed envelope, as seen in Figure 2.10.

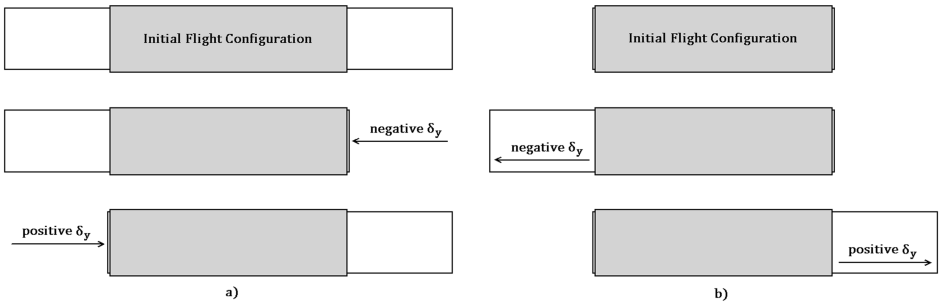

Figure 2.9 Wing deflection variable for: a) Flight with wings extended, below 20 m/s; b) Flight with wings retracted, above 20 m/s

As studied by *Gamboa et al.* [23] two years ago, the vehicle's speed efficiency in relation to wing span shows that the best flying condition is wings fully extended. For higher velocities, the most efficient scheme is wings fully retracted. This created a need of two distinct flying

modes, as shown in Figure 2.9. The code was written considering the airplane is flying levelled with wings fully extended, which refers as Figure 2.9 a) for the related wing deflections signals.

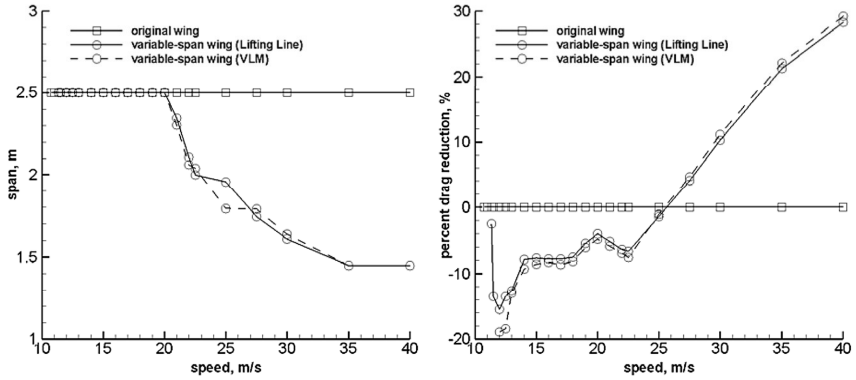

Figure 2.10 Span variation with flight speed (left) and drag reduction relative to original wing (right) for the original and variable-span wings [23].

The full wing chord varies between 280 millimetres on the root to 250 millimetres on the tip, as the moving wing is narrower relating to the main fixed wing [23] (see Figure 2.5 and images annexed). To minimize the analysis error due to this small "step" between wings, the simulations were performed using the M.A.C. (*Medium Aerodynamic Chord*) of 270 millimetres. As such, the resulting data constants to be applied in the flight equations are:

Table 2.4 Aircraft and flight conditions data

Take-off weight: $6.700\ \mathrm{kg}$	Altitude: $0\ \mathrm{m}$ (Sea Level)
Span (maximum span): $2.500\ \mathrm{m}$	Flight speed: $20\ \mathrm{m/s}$
Wing median chord: $0.27\ \mathrm{m}$	Engine traction: $25\ \mathrm{N}$ (assumed)

The inertial moments were assumed from previous calculations at project phase of "Olharapo" at *Universidade da Beira Interior* [25] and are present in Table 2.5. This was done due to the complexity of new calculations and also because this new configuration is still in testing, as the aircraft configuration has not changed much. The values obtained in XFLR are similar to those in Table 2.5.

Table 2.5 Inertial moments assumed

$I_{xx} = 0.617\ \mathrm{kg \cdot m^2}$	$I_{yy} = 0.341\ \mathrm{kg \cdot m^2}$	$I_{zz} = 0.935\ \mathrm{kg \cdot m^2}$	$I_{xz} = 0.037\ \mathrm{kg \cdot m^2}$

With this data we have the necessary conditions to project a controller, as nothing else needs to be estimated. These values are subject to change as the UAV is still under development and testing, but the obtained derivatives are already very close to those that would be found with a full *wind-tunnel* or *in flight* analysis.

Chapter 3

Simulation and Tests

In order to fully demonstrate and test the validity of a controlled dissymmetrical span system described in this work, the following analysis was made using MATLAB [26] software. Taking full use of the mathematical and programming tools provided, the simulation of a control response after a disturbance or equilibrium change was applied with ease.

The working scheme of this system is not a conventional one. As such, some considerations must be made when writing the code. At this point it is important to notice that most of the programming bases used were developed during stability and control classes one year before this work. As such, most of the code had to be simplified and adapted to comply with this one's objectives.

3.1 Imposed Flying Qualities

On Chapter 1 the resumed theory behind flying qualities was described (equations 1.51 to 1.55). To apply these values in control, the theory developed by *Jia Luo and C. Edward Lan* [16] (also already resumed in Chapter 1, equations 1.62 to 1.66) was followed and these are inputted in the vector λ for Q matrix estimation. When using the eigenvalues given by the characteristic equation of the state matrix A, the controller stabilizes but only after a certain time, considering the tested airplane to be controllable and stable in flight. For a difficult to control vehicle, or unstable on some flight mode, this will not result in an optimal controller, as no optimization is actually performed. As such, by inverting the determination of the flying qualities to predetermined data, which was set as Level 1, Class I, Cat. B airplane (Cat. B because it is most adequate for the type of vehicle and missions, see annexes), the corresponding optimal values to apply in vector λ were then found easily. This predetermined data is found along various books [4] [5] [7] and was also annexed to this work. To accomplish this, the frequency and damping equations were solved in order to the real and imaginary parts of each value.

For each motion theory, the corresponding values for a Level 1, Class I, Cat. B airplane are all resumed in Table 3.1:

Table 3.1 Level 1, Class I, Cat. B corresponding parameters for each flight mode

	ω_n	ξ	$\xi \cdot \omega_n$	T_2	T_t
Short − period	0.4 to 0.6	0.5 to 0.9	−	−	−
Long − period	−	> 0.04	−	< 55 s	−
Spiral	−	−	−	> 20 s	−
Dutch roll	> 0.4	> 0.08	> 0.15	−	−
Roll	−	−	−	−	< 1.4 s

The short-period oscillation parameter limits were obtained from Figure 3.1. As can be observed, the best controllability and responsiveness is obtained inside the *Satisfactory* area of the graphic.

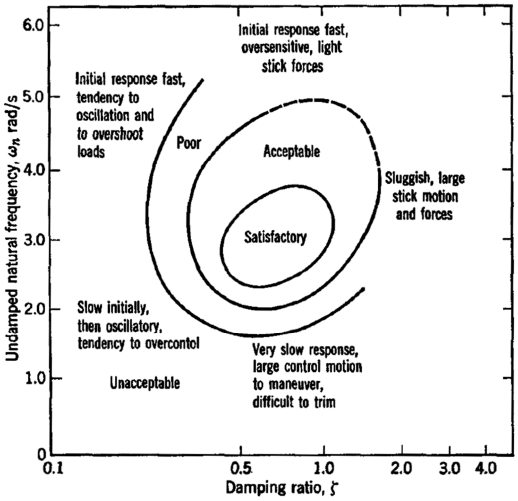

Figure 3.1 Short-period parameters from pilot opinions [6]

All other values for each remaining flight mode were obtained from the equations written in Chapter 1 (equations 1.51 to 1.55), solved in order to the real and imaginary parts and using the data from Table 3.1. For the oscillatory modes (long period, Dutch roll), where the complex form $\lambda = a \pm bi$ is used, the following real and imaginary parts of the eigenvalues were determined (as in equation 1.52) from equations (3.1) and (3.2):

$$a = -\xi \cdot \omega_n \tag{3.1}$$

$$b = \omega_n \sqrt{1 - \xi^2} \tag{3.2}$$

The eigenvalues for the two non-oscillatory modes (spiral and roll) need to be obtained from equations (1.54) and (1.55), simply solving in order to the Eigen value from equations (3.3) and (3.4), respectively:

$$\lambda_s = -\frac{\log(2)}{T_2} \tag{3.3}$$

$$\lambda_r = -\frac{1}{T_t} \tag{3.4}$$

Replacing the variables with values from Table 3.1, it is possible to obtain the optimal Level 1, Class I, Cat. B eigenvalues that are imposed in control, allowing an also optimal Q matrix. The values used are present in Table 3.2 below:

Table 3.2 Variables chosen for Eigen value calculation

	ω_n	ξ	$\xi \cdot \omega_n$	T_2	T_t
Short − period	3	0.75	−	−	−
Long − period	−	0.40	−	10 s	−
Spiral	−	−	−	23 s	−
Dutch roll	0.60	0.70	0.42	−	−
Roll	−	−	−	−	0.10 s

The vector composed of all these calculated eigenvalues (eigenvector) which is used in control is given by:

$$\begin{gathered} \lambda = [\lambda_{sp\ 1,2} \quad \lambda_{lp\ 1,2} \quad \lambda_r \quad \lambda_{dr\ 1,2} \quad \lambda_s] \\ = \\ \lambda = [-2.25 \pm 1.9843i \quad -0.0693 \pm 0.1588i \quad -10.0 \quad -0.42 \pm 0.4285i \quad -0.0301] \end{gathered} \tag{3.5}$$

Three simulations were performed to completely prove the working concept of this unordinary but robust system controller.

3.2 Classical Control Method (Disturbance Response)

When designing a controller for a specified vehicle (or system, i.e. damper, spring and mass), there are two main approaches to be taken: frequency domain and time domain. In the first technic there are open-loop and closed loop systems. In open-loop designs the control action (input) does not depend on the output, where in closed-loop systems they are dependant (feedbacked), increasing accuracy [7]. The design for a frequency domain controller is based on transfer functions (*Laplace* transforms) for each control component, and the root locus technic for finding the best roots of the characteristic equation (eigenvalues), which tends to be a trial-and-error method with lots of calculations performed. For large control systems implementation, this gets very complex.

The applied control method is the most modern nowadays (modern control theory). This is a time domain method, where the control variables are described by several first-order differential equations, easily solved using a computer. As described in Chapter 1 (1.56 to 1.67), the first implemented method is built using the LQR control theory.

The most classic method to analyse is the simulated state variable response for an atmospheric disturbance of the trimmed control surfaces, in order to return all state variables to the previous equilibrium point. As such, to accomplish this, a code was written following the order in Figure 3.2, where all parts were already explained in detail along previous chapters.

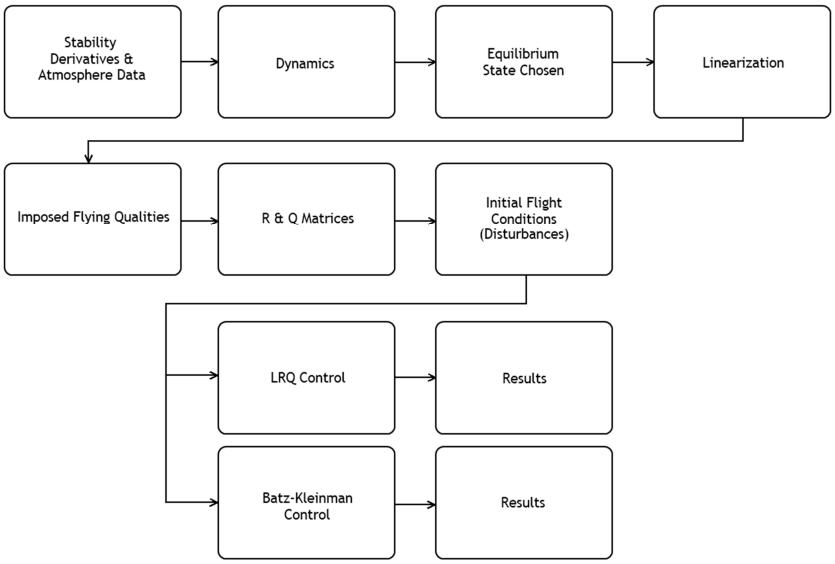

Figure 3.2 Diagram of program simulation flow scheme (in general)

The disturbance can be defined by a uniform fractioned divergence from the equilibrium state variables defined before, or by inputted values from the user. The equilibrium is obtained by linearizing the system using, for example, *Taylor's* equation [5]. This first simulation, as well as the following, is performed at sea level altitude and a cruise speed of 20 m/s, at levelled flight, from Table 2.4. The equilibrium state and control variables obtained from solving $f(x_{eq}, u_{eq}) = f(x_0, u_0) = 0$, which gives the results found in Table 3.3 and Table 3.4.

Table 3.3 Equilibrium State constants

$u = 20$ m/s	$w = 0$ m/s	$q = 0$ rad/s
$\theta = 0.0481$ rad	$v = 0$ m/s	$p = 0$ rad/s
$r = 0$ rad/s	$\phi = 0$ rad	$\psi = 0$ (not considered)

Table 3.4 Equilibrium Control constants

$\delta_{V_e} = -0.0180$ rad	$\delta_T = 16.89\%$	$\delta_y = 0$ m	$\delta_{V_r} = 0$ rad

The state and control vectors are then defined as:

$$x = \begin{bmatrix} u \\ w \\ q \\ \theta \\ v \\ p \\ r \\ \phi \end{bmatrix} = \begin{bmatrix} 20 \\ 0 \\ 0 \\ 0.0481 \\ 0 \\ 0 \\ 0 \\ 0 \end{bmatrix} \quad \text{and} \quad u = \begin{bmatrix} \delta_{V_e} \\ \delta_T \\ \delta_y \\ \delta_{V_r} \end{bmatrix} = \begin{bmatrix} -0.0180 \\ 0.1689 \\ 0 \\ 0 \end{bmatrix} \tag{3.6}$$

Note that the levelled flight condition is achieved with 17% power and a small positive pitch of about $2.7\ \mathrm{deg}$, which is maintained with a negative elevator (nose up) deflection of about $1\ \mathrm{deg}$. For this work, and so that the aircraft is not excessively perturbed, small disturbances to every state variable were applied. Two separate cases were studied in order to provide enough prove of work. As such, the disturbances vectors ($x_1$and x_2) to apply in the LQR and Batz-Kleinman calculation are:

$$x_1 = \begin{bmatrix} 22 \\ -2 \\ -0.03 \\ 0.0181 \\ 2 \\ 0.03 \\ 0.03 \\ 0.03 \end{bmatrix} \text{ and } x_2 = \begin{bmatrix} 18 \\ 2 \\ 0.03 \\ 0.0781 \\ -2 \\ -0.03 \\ -0.03 \\ -0.03 \end{bmatrix} \tag{3.7}$$

This represents, for x_1:

- an increase in all tree velocity components ($u = 22\ \mathrm{m/s},\ w = -2\ \mathrm{m/s}$ and $v = 2\ \mathrm{m/s}$), where the vertical velocity w is negative for a climb (z vector is pointing down as seen in Figure 1.5) and the lateral velocity v is positive for moving to the right;

- a positive rate of variation for lateral-directional roll and yaw components ($p \text{ and } r = 0.03\ \mathrm{rad/s}$), meaning the aircraft is rolling with right wing down, and yawing to the right, respectively;

- a negative rate of variation for longitudinal pitch component ($q = -0.03\ \mathrm{rad/s}$) meaning the aircraft is pitching up (nose up).

- a positive pitch angle $\theta = 0.0181\ \mathrm{rad}$, meaning initially a nose up angle $0.03\ \mathrm{rad}$ below equilibrium, and a positive bank angle $\phi = 0.03\ \mathrm{rad}$, that represents banking right wing down.

For the second simulation (x_2) the used disturbances are symmetric to those in x_1, the exception being the pitch angle, which now is $\theta = 0.0781\ \mathrm{rad}$, meaning a nose up $0.03\ \mathrm{rad}$ above the previously calculated equilibrium value in (3.6).

One other aspect to notice is that the initial control values used are the equilibrium values calculated, so to simulate the aircraft is flying at levelled cruise before the disturbance occurs.

The objective of this simulation is that the controller fully stabilizes in about 6 seconds. Running both simulated initial conditions and with the imposed Level 1 handling qualities, the UAV is then able to return to its equilibrium state, as observed in Figure 3.3 (for first disturbance vector x_1) below:

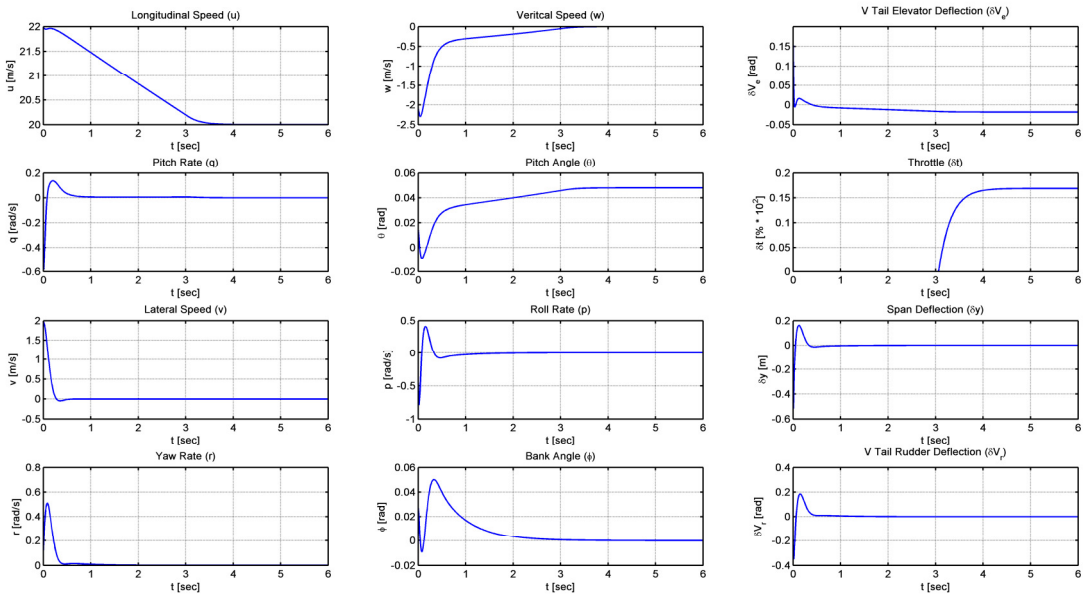

Figure 3.3 Classic disturbance simulation response with LQR for x_1

For the Batz-Kleinman controller, there is no influence from the imposed eigenvalues, thus as seen in Chapter 1, this control method differs from the LQR method by a small number of parameters. This controller relies on the calculation of the P matrix from solving the *Gramian* integral in (1.69). The only optimizing data is the number of intervals for the integral estimation (n), which was set at $n = 400$, and the final integration value τ, set at $\tau = 0.3$. Higher values of τ provide a more oscillating stabilization, as the integral limits start to diverge from the linearized boundaries. The remaining simulation data was the one used for the LQR method, and the UAV stabilizes in a similar way as before (Figure 3.4):

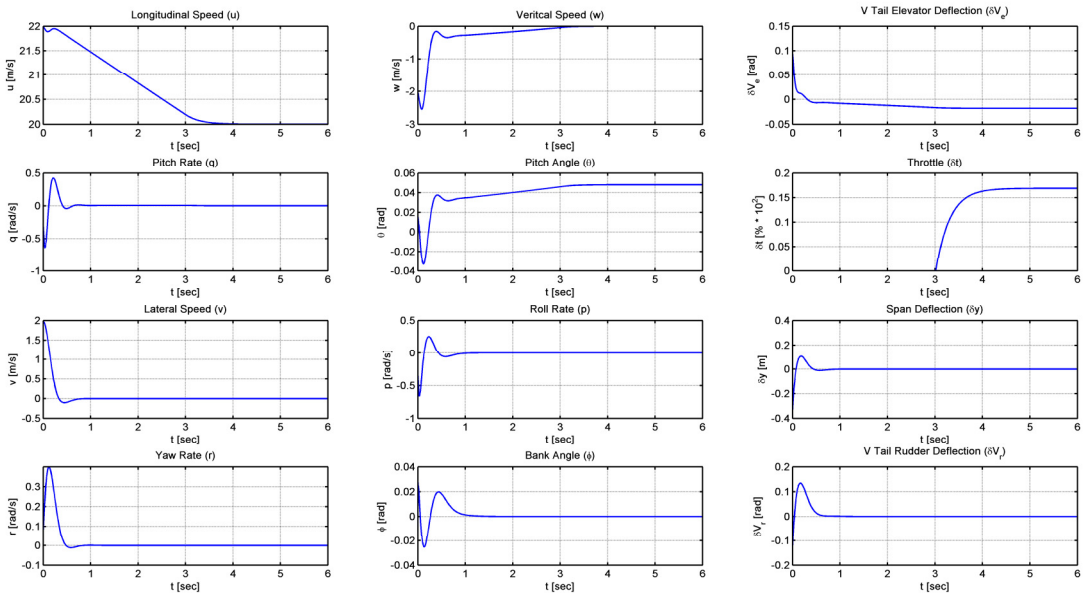

Figure 3.4 Classic disturbance simulation response with Batz-Kleinman for x_1

Analysing in detail only the variables respective to roll control, the bank angle, roll rate and span deflection variations are joined in two graphics, one for each method for the first simulation x_1 (Figure 3.5):

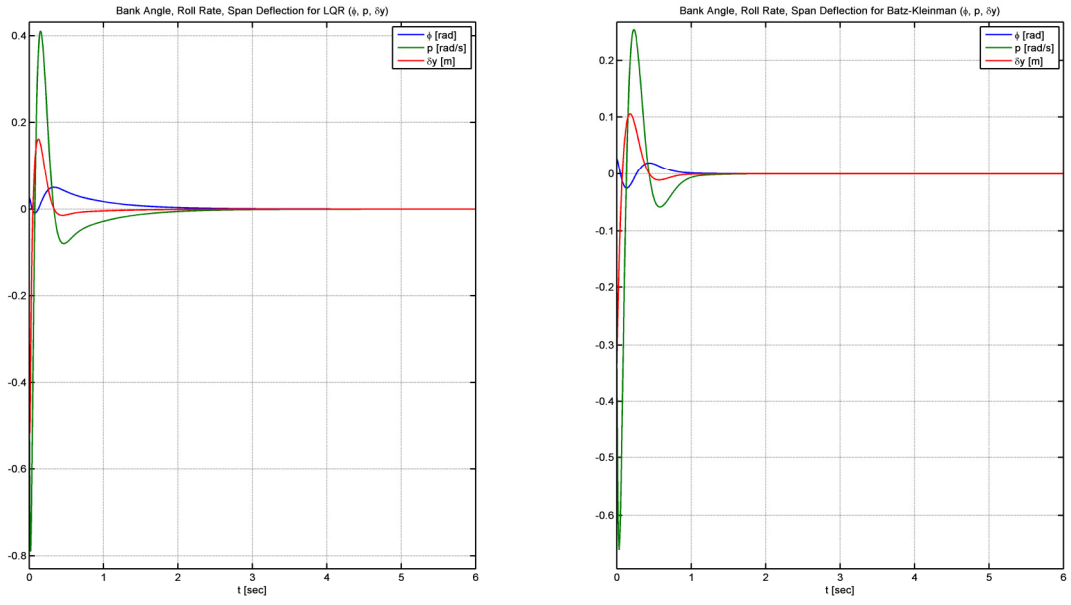

Figure 3.5 Detailed roll control and state variables for classic simulation with LQR (left) and Batz-Kleinman (right)

As can be seen, both methods stabilize in less than 3 seconds, being Batz-Kleinman's the most efficient (energy wise, and time wise), but also very hard on control actuation for smaller values of τ. As the Q matrix was dimensioned assuming a very responsive and stable airplane (Level 1, Class I, Cat. B) the LQR control data is also very smooth. If the original eigenvalues

of the state matrix A were used, this would not be alike, and 6 seconds might not be enough for a full stabilization.

The simulations were performed for a very small disturbance of the bank angle (as well as other variables) and the dissymmetric variation of the wings for control can be recognized in Figure 3.5, as expected. The wing control system uses about $1/6$ of its maximum deflection for LQR and $1/10$ for Batz-Kleinman's (seen in red in Figure 3.5). This is normal as the 4 control variables intervene on the stabilization, and the V-Tail is sufficient to stabilize the UAV roll moment. Here it is not easy to see, but for a positive bank angle rate (Roll rate) a negative deflection of the wing is induced to force a return to zero (equilibrium) conditions. To prove the system is controllable for different disturbances, the second simulation x_2 values can be observed in Figure 3.6 and Figure 3.7 below.

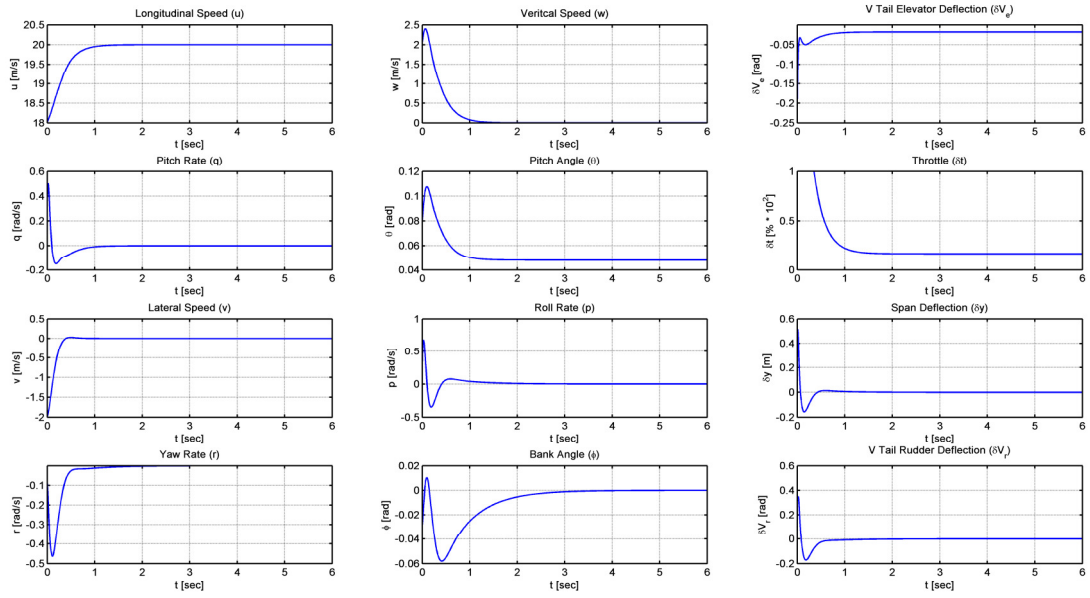

Figure 3.6 Classic disturbance simulation response with LQR for x_2

This new simulation, as previously described, is the reverse of the first. As can be realized, both control methods return to initial equilibrium conditions in less than 3 seconds as before, even for a completely opposite disturbance, proving that the controller is well dimensioned. Once more the influence of the control variables is noticed, and the Batz-Kleinman's is also the most effective.

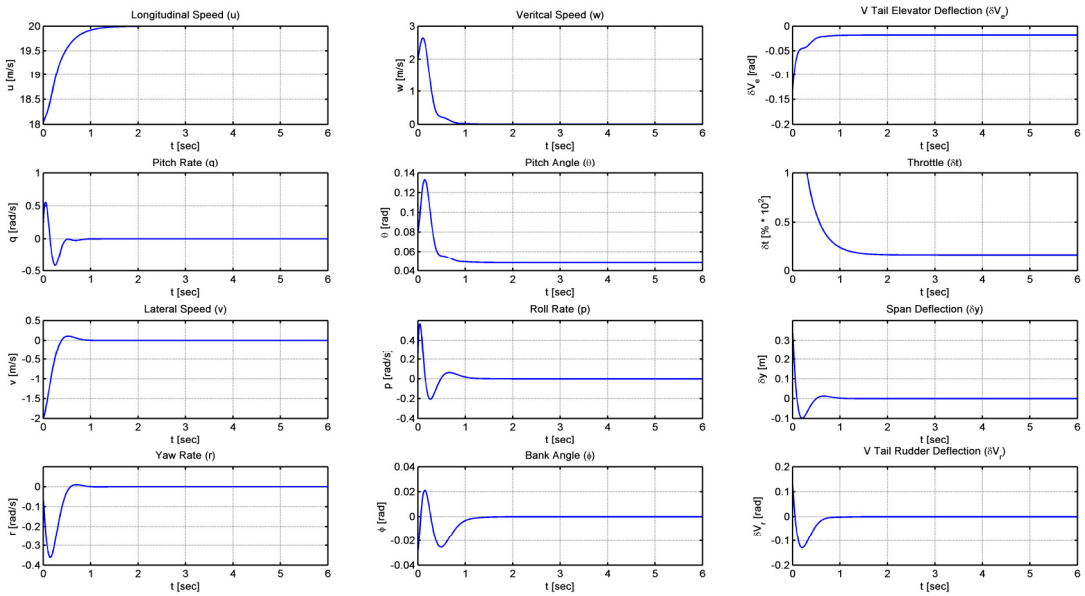

Figure 3.7 Classic disturbance simulation response with Batz-Kleinman for x_2

Another interesting simulation that could be performed is a random variation of disturbance vectors, that simulate a very unpredictable flight condition, where the UAV is under a great amount of stress. If a convergence is noticed for a given time span between values, than the controller's efficiency can be proved.

3.3 Bank Angle Sinusoidal Variation

On the classical simulation the relationship between the induced control and consequent reaction in state variables was not easy to see. As such, a more complex analysis was performed. For this simulation, a large number of equilibrium states were calculated, varying only the bank angle ϕ with a sinusoidal function in order to force the UAV to perform a variable turn to, i. e., avoid an obstacle such as a tree or building. The maximum bank angle was set to 30 degrees. The remaining data used before is also inputted here, and the imposed flight qualities used are the same for each equilibrium state (which is an approximation as the bank angle is reduced). Every fixed number of seconds the UAV changes its bank angle and a new equilibrium point and controller is dimensioned. The objective is to force the airplane bank angle in order to deflect both wings as much as needed, thus making it possible to see the reactions of state and control variables and proving the concept mechanism works. For this two different time span simulations (y_1 and y_2) were calculated for 6 and 3 seconds between equilibrium points respectively, as will be described later. To induce a full smooth symmetric amplitude in bank, the bank angle ϕ follows the curve in Figure 3.8:

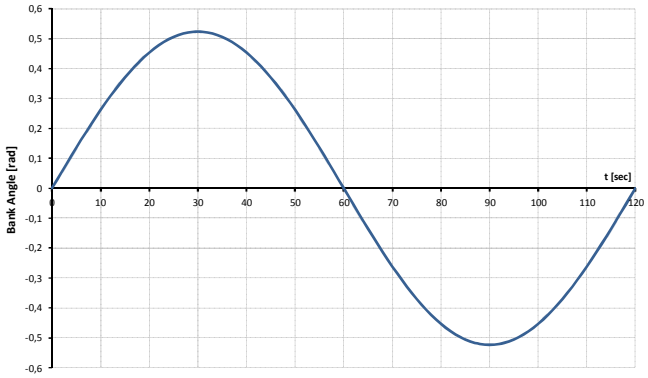

Figure 3.8 Sinusoidal variation of the bank angle (maximum bank 30 degrees, time 120 seconds, for y_1)

This represents the following equation:

$$\phi = \frac{|\phi_{max} - \phi_{min}|}{2} \cos\left[\left(\frac{2\pi}{(t_{max} - t_{min})}\right)\left(t + \frac{3}{4}(t_{max} - t_{min})\right)\right] \quad (3.8)$$

The total time in the figure is 120 seconds, and a number of 20 equilibrium points were calculated (for 20 bank angle positions). This simulation (y_1) was run for a total time of $\left(120 + \frac{120}{20}\right) = 126$ seconds to enable a return to the initial values, meaning a time of 6 seconds between equilibrium points. For the second simulation (y_2), the total time is reduced in half to 60 seconds (the number of equilibrium points is the same), and the time between values is also half, 3 seconds. The first (y_1) obtained results follow the bank sinusoidal distribution as can be observed in Figure 3.9 for the LQR implementation and in Figure 3.10 for Batz-Kleinman. In Figure 3.9 a small deflection of right and then left wings is observed as the curve angle is increased to maintain a maximum bank of 30 degrees in both directions. Each 6 seconds of simulation the angle varies and forces the controller to move to the next equilibrium point, always considering the previous stable (or nearly stable for the small stabilization time) variables for state and control as the initial values used next. Previous classic control method results did not evidence the controller response to each change of attitude as can be seen here. Positive and negative responses that indicate the airplane position in space are now observed fully. As the bank increases, the aircraft is more stressed, and to maintain this flight condition the control variables suffer an increase in variation. The span variation is opposite in signal to the bank angle, which had been acknowledged with the description of the system in Chapter 2. Notice also that the longitudinal angle of pitch is increased positively as the bank increases in order to maintain a levelled turn, which is maintained by a negative deflection of the V-Tail elevator equivalent. The rudder control surface suffers an inversed but similar variation with span deflection that proves the interaction between *ailerons* (here as wing span dissymmetry) and V-Tail rudder equivalent, as a negative variation of the rudder induces a positive yaw angle.

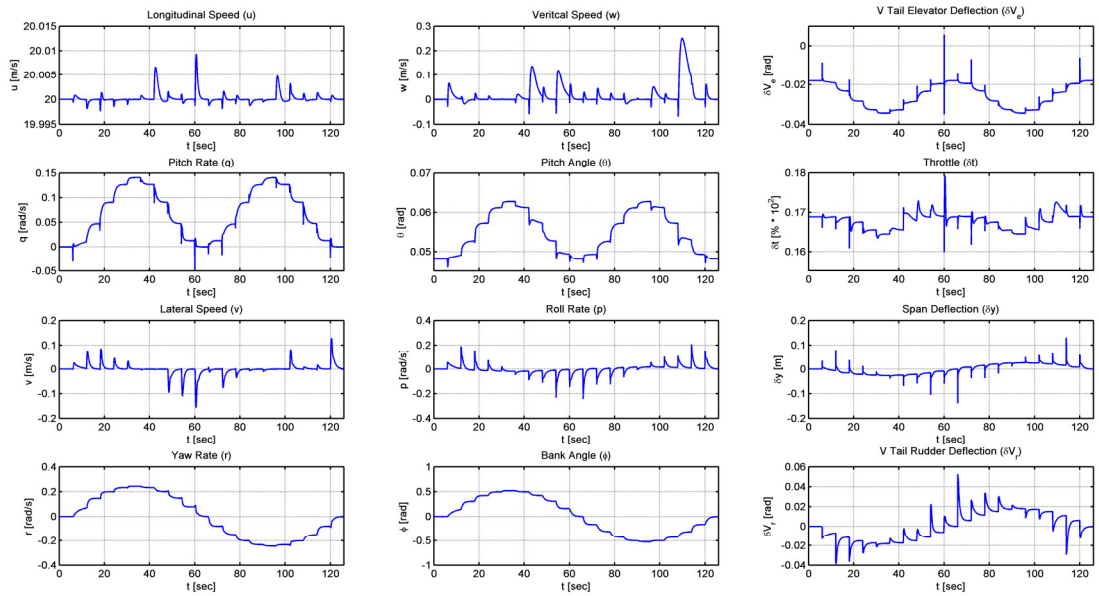

Figure 3.9 LQR simulation for a sinusoidal variation of bank for y_1

In the velocities graphics there are some strange sudden changes in amplitude mainly during a reduction or increase in bank, which is due to the imposition of non-optimized eigenvalues and may be ignored as do not influence in control. For the Batz-Kleinman control method used, the results observed in Figure 3.10 are much the same as with the LQR method, without these variations in velocity as no weight matrices are needed. Small differences occur as seen before in smoothness, stabilization time, and energy use, that can be observed and compared better in Figure 3.11, as the Batz-Kleinman is much faster to stabilize than the LQR.

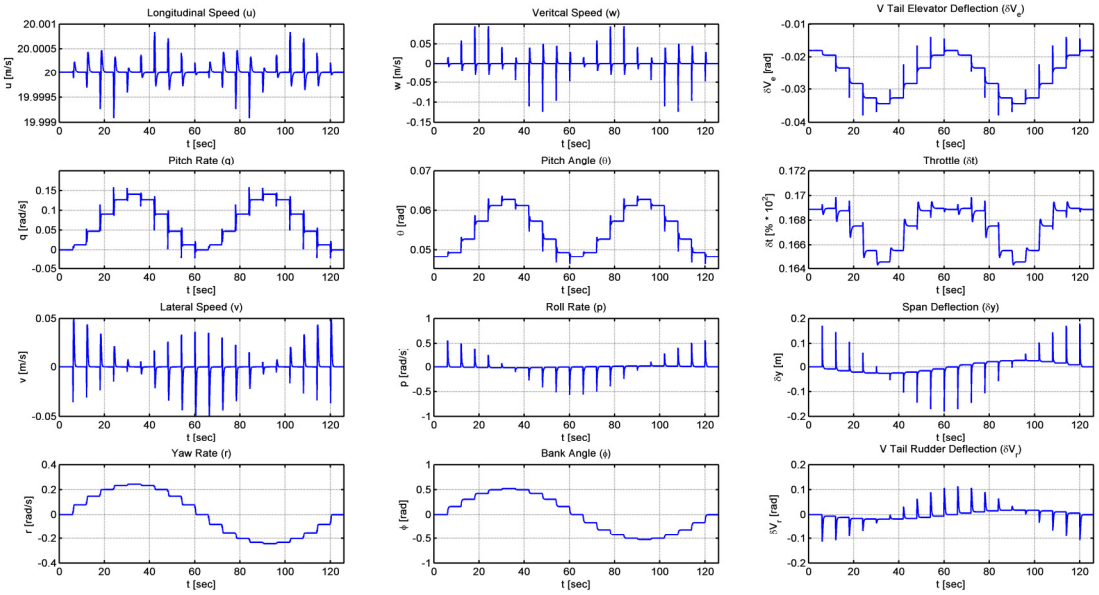

Figure 3.10 Batz-Kleinman simulation for a sinusoidal variation of bank for y_1

From Figure 3.11 the two methods are put side-by-side the same way as in Figure 3.5. By comparing in detail the three roll related variables shown, it is also observable that the influence of bank angle on wing span variation is inverted, as a negative wing deflection (in red, corresponding to a retraction of the right wing below $20\,\mathrm{m/s}$ as seen in Chapter 2) is needed to maintain a positive bank angle (in blue, rolling right). For a bank of 30 degrees the wing deflects no more than a few centimetres. The roll rates (in green) are distributed in a shifted phase related to the bank angle: the smaller the change in bank, the smaller the needed roll rate. For a positive change of bank, a positive rate is observed as would be expected, as for an almost null rate when at maximum bank.

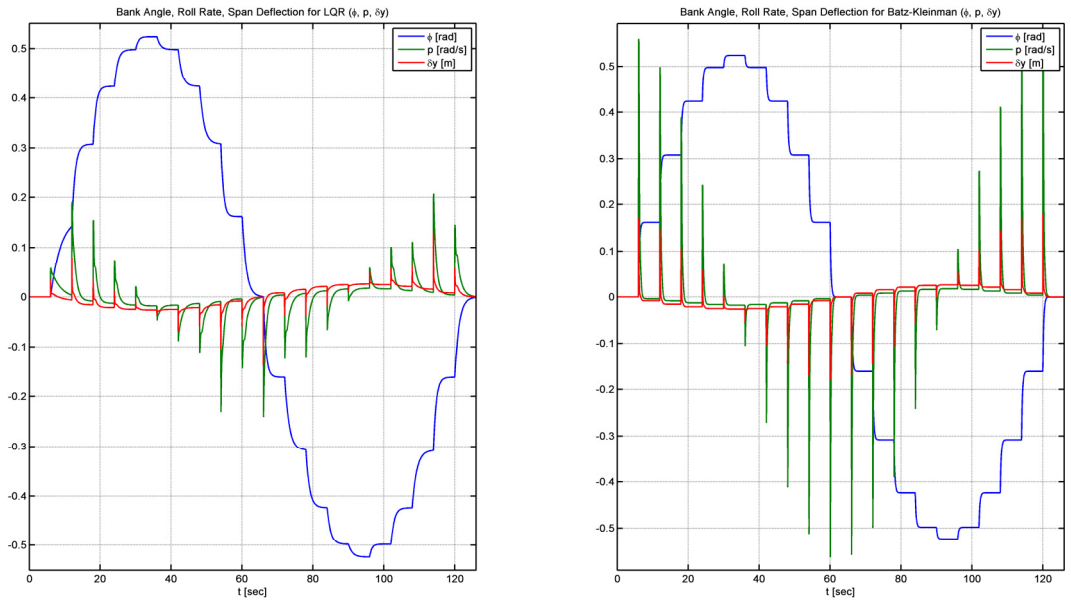

Figure 3.11 Detailed roll control and state variables for sinusoidal simulation with LQR (left) and Batz-Kleinman (right) for y_1

As seen, the system stabilizes for every equilibrium point in less than 6 seconds. To see what happens if this time span is reduced, the same analysis was made now for 3 seconds of time. For the LQR control method in Figure 3.12, the instabilities increase as expected. More small disturbances in velocity and other variables occur, but, as before, the response of the controller is not influenced. The main aspect to notice is the steeper “saw tooth” changes in roll rate and wing deflection, where the roll rate never fully returns to equilibrium between bank variations. In Figure 3.14 this is well acknowledged, and a comparison between the two control methods can also be seen.

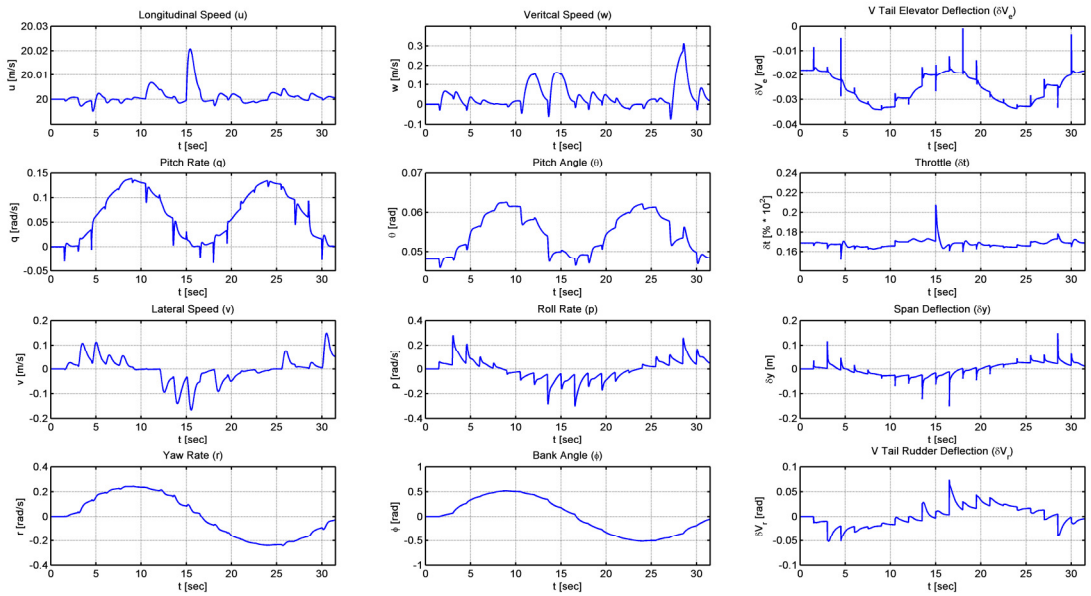

Figure 3.12 LQR simulation for a sinusoidal variation of bank for y_2

The maximum bank angle in LQR is not completely achieved (Figure 3.12 and Figure 3.14). For a smaller time span, the controller would not be able to keep up with the different equilibrium changes. The Batz-Kleinman is much more efficient as already noticed, and is now even more acknowledged in Figure 3.13 as every variable is stabilized quickly. It is also much hard on the UAV, as roll rates for instance are doubled in relation to LQR (observed in Figure 3.11 and Figure 3.14).

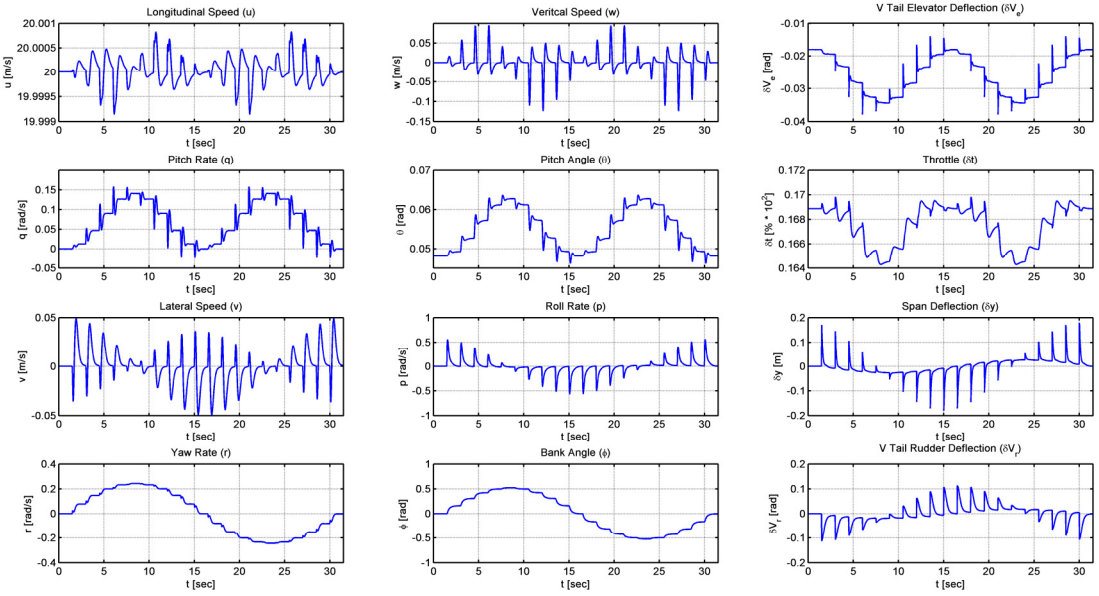

Figure 3.13 Batz-Kleinman simulation for a sinusoidal variation of bank for y_2

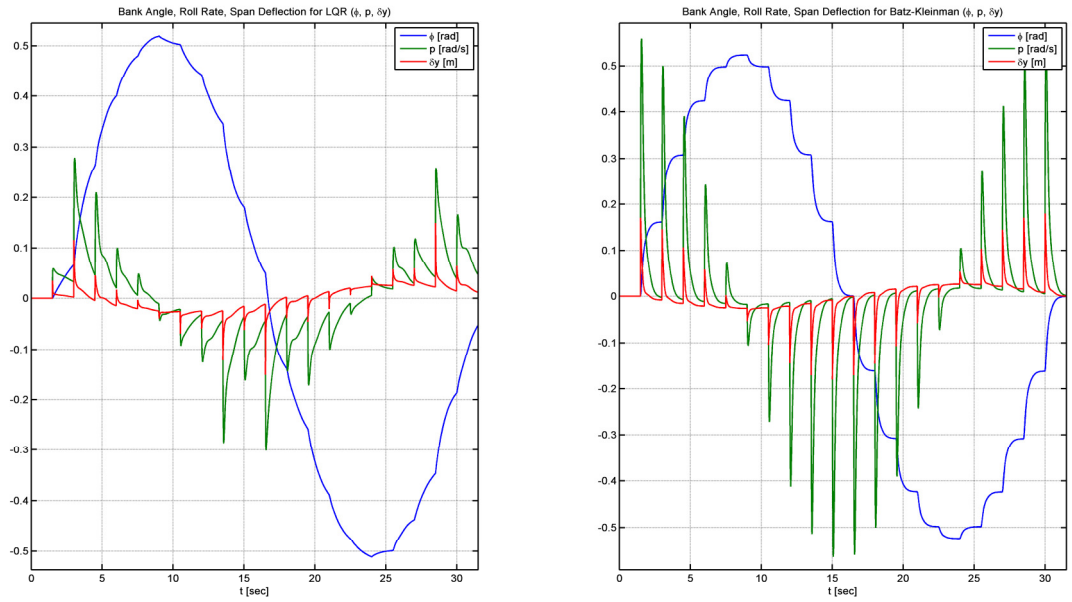

Figure 3.14 Detailed roll control and state variables for sinusoidal simulation with LQR (left) and Batz-Kleinman (right) for y_2

Both this and previous (Classical) analysis describe and validate this working concept. The two control methods implemented and simulated cases also allow a fairly decent bank analysis for smooth conditions. A last simulation was run based on this last, but instead of a sinusoidal variation of bank, a random two step maximum bank and subsequent equilibrium state was used. This allows a simulation of very unusual flight conditions, as the airplane does no fly straight and levelled for more than 6 and later 3 seconds at a time.

3.4 Random Bank Angle Variation (Two Step Maximum)

For this simulation the same code used in (3.8) was implemented, as well as the same equilibrium states. The difference lies in the controller simulation, as for the first simulation (z_1) every 6 seconds the program chooses a random point, no more than two steps above or below the previous equilibrium value. For the second simulation (z_2) the time changes to 3 seconds. As the same conditions and determined variables were used, the stabilization aspect for each equilibrium state is equal to that seen in the last one. Two simulations for the same time span values as previous example were implemented, but only one control method was studied, the LQR, due to being the hardest to stabilize and so the best to analyse. The random variable that determines the next equilibrium was created using only MATLAB's [26] commands.

Running the code with these random values for simulation z_1 returned the following results present in Figure 3.15.

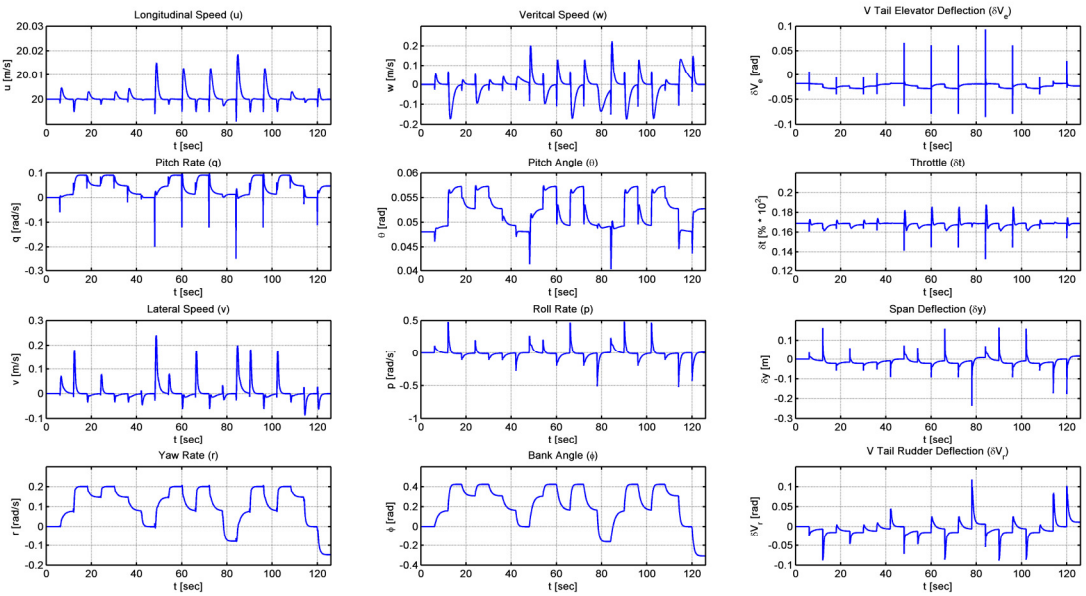

Figure 3.15 Random bank simulation using LQR for z_1

A random simulation of this kind is representative of a constant change in direction due to the bank variation and respective change of turn. For this analysis, the main aspect is the ability of the airplane to stabilize given an unknown next equilibrium state. The response of wing deflection due to bank is shown in detail in Figure 3.16, which is similar to previous simulations except to the fact that every 6 seconds an unknown bank is used.

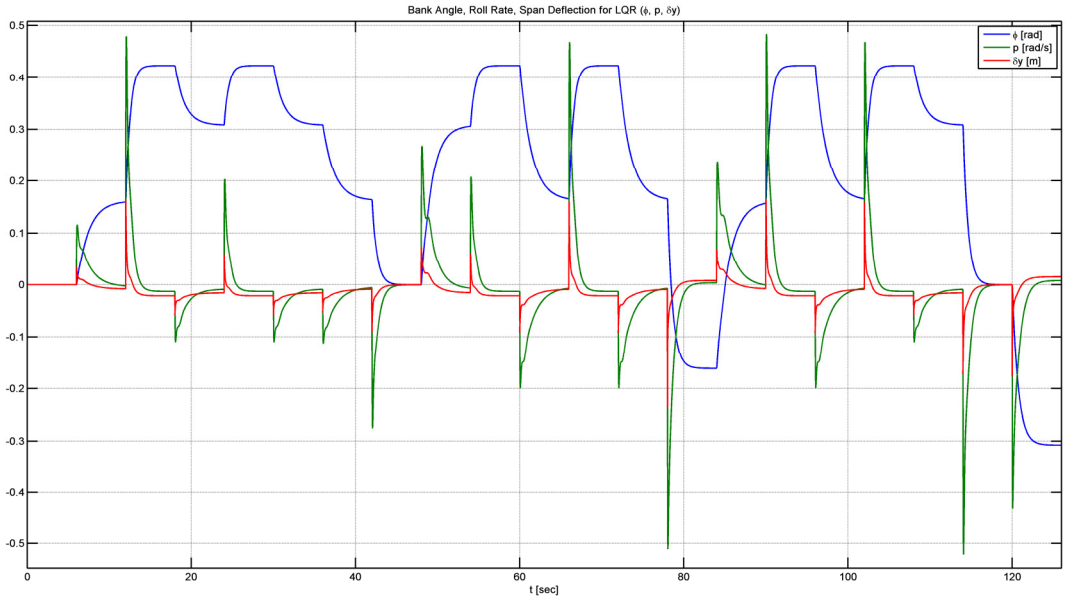

Figure 3.16 Detailed roll control and state variables for random simulation with LQR for z_1

A return to original wing levelled state is seen twice during the simulation, but is not relevant. One main consideration to take is the amplitude of the random values, which is not

greater than 2 steps in order to keep the bank angle changes inside this given limit of no more than 2 angles above or below the previous value. If these limits were not imposed, the controller may not have time to stabilize bank or other variables during the time intervals. Reducing the time intervals to 3 seconds between equilibrium changes (z_2), the roll related variables response is seen in Figure 3.17. The random values are not the same as before, to simulate other conditions. Other variables were omitted in this last analysis, as the differences are well observed.

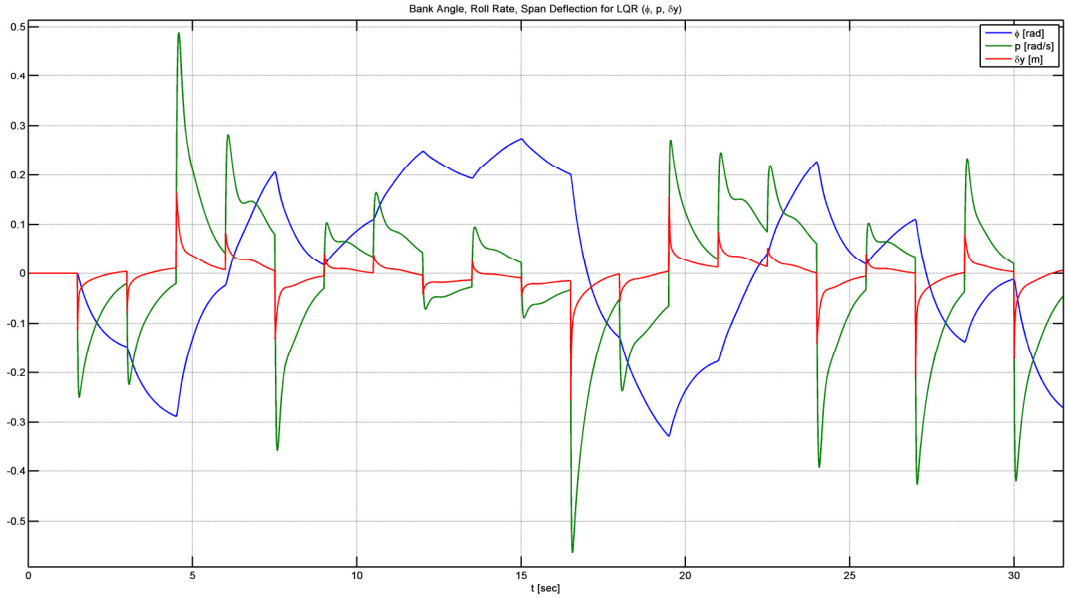

Figure 3.17 Detailed roll control and state variables for random simulation with LQR for z_2

As seen before in Figure 3.14 the system do not have enough time to fully stabilise, thus appearing as a “saw-toothed” line. Even so, there are no divergences or loss of control even for these unstable and unpredicted simulation values, proving the control system is indeed robust. There is a compromise between a very long-lasting but smooth convergence and a short timed and hard stabilization. A smooth one is preferred for optimal flight conditions and a big aircraft, opposed to a hard control that is best used in very demanding flight conditions where a fast stabilization is needed in order to minimize off-course divergences. Both controller methods are subject to further optimizations, as both allow a “tuning” to comply with required conditions. The LQR is more tolerant to this as there are various aspects than can be optimised but requires much more analysis time to adjust them. The Batz-Kleinman is less open to optimizations, but is the most reliable, control wise. Other methods also deserving of notice exist nowadays [5] [17].

Chapter 4

Conclusions

The main aspect of this work was the design and validation of a controller for a new morphing wing system. This new system is to be applied on a UAV projected and built at *Universidade da Beira Interior*, which has been under development over the last two years [23]. As it is not an ordinary system, it required some thorough analysis. A variable-span dissymmetric morphing wing mechanism allows, as explained over this work, the full replacement of the standard aileron system. The moment created around the longitudinal axis of the airplane is now done by the differential pressure from the change in wing span. The main objective of this system is the reduction of drag with wing deflection for roll and for leveled cruise, when flying with both wings retracted, enabling a longer cruise and faster speed. As it requires a more complex building process and heavier parts, it is a valuable challenge.

The implementation of a controller to stabilize the roll motion of the airplane automatically after a disturbance or to follow specified equilibrium points is the main focus of this work, not only to perform roll control, but also to stabilize every other flight variable. This allows a fully operational controller.

Along with a revision of the dynamics of an airplane and response to control surface deflections, the flying qualities theory was also studied. As from the data retrieved with XLFR and the real airplane data, the quality levels were not optimal, and an experimental new method [16] for integrating the required eigenvalues using the LQR controller was implemented. This enabled a more complete optimization of the resulting LQR controller.

Two control methods were tested, LQR and Batz-Kleinman controller, and to validate the two, three main different simulations were performed. A classic disturbance and controller response illustrated the good stability convergence to equilibrium values, occurring before five seconds of simulation time. The simulation was repeated to different disturbance values to test and validate the robustness of the controller. Both methods proved to work equally fine, being the LQR the only optimizing one by tempering with the weights matrices. The Batz-Kleinman method originated the best results with the faster convergence. The use of the variable-span system also proved to work well, but is not easily seen with this simulation. For a complete understanding of how the wing retraction/extension system responds to a turn, and the effects in all other longitudinal and lateral variables, a new simulation was done. Here instead of a single equilibrium state, a large number of sequentially collocated points along a sinusoidal curve were implemented. As such, every given constant variation in time,

the controller stabilizes for a different equilibrium, being possible to choose which equilibrium state we want by altering the roll angle. As before, two different simulations were performed, here for two different time spans. By the data obtained from this simulation, and only analyzing the roll motion, in Figure 3.11 it is noticeable the similarity between the variable-span and *aileron* systems in control purposes. A positive bank angle is maintained by a negative deflection of a wing, meaning the right wing retracts when flying with both wings extended, or the left wing extends for the opposite flying configuration. This similarity is what makes this system good to implement, as for a pilot, theoretically the airplane controls are the same.

A third simulation was made to analyze the influence of a random variation of the same bank related equilibrium points used. To this simulation the results show that the airplane responds well to every variation, stabilizing always in less than the differential time used between each change.

In all the simulations the best results were achieved with the Batz-Kleinman control method. The LQR method also performed well, but is not as smooth when comparing both controllers. The main aspect of the last is that it can be greatly optimized and tweaked.

In general the airplane responded very well to every disturbance forced and every change in bank angle, proving this new concept works, in theory of course. A real system needs to take in account many other adverse aspects that worsen the flying motion and control, such as vibrations, lag in servos, interference, and weather conditions at the time.

The design, optimization and testing made were possible due to the previous work done by my supervisors.

With my work, only the surface was touched along a tedious implementation of a fully working controlling system. Indeed, further work needs to be developed to allow the physical integration of a real autopilot system on the UAV, as well as thorough testing procedures to ensure that nothing goes wrong in-flight.

Bibliography

[1] Wright Brothers History, http://www.wright-house.com/wright-brothers/wrights/1903, (17-10-2011).

[2] M. J. Abzug and E. E. Larrabee, *Airplane Stability and Control*, Second Edition ed. United Kingdom: Cambridge University Press, 2002.

[3] B. N. Pamadi, *Performance, Stability, Dynamics and Control of Airplanes*. United States of America: American Institute of Aeronautics and Astronautics, Inc., 1998.

[4] D. McLean, *Automatic Flight Control Systems*. Reino Unido: Prentice-Hall International, 1990.

[5] B. D. O. Anderson and J. B. Moore, *Linear Optimal Control*.: Prentice-Hall, 1989.

[6] B. Etkin and L. D. Reid, *Dynamics of Flight Stability and Control*. United States of America: John Wiley & Sons, Inc., 1996.

[7] R. C. Nelson, *Flight Stability and Automation Control*. United States of America: McGraw-Hill, 1989.

[8] B. L. Stevens and F. L. Lewis, *Aircraft Control and Simulation*. United States of America: John Wiley & Sons, Inc., 1992.

[9] XFLR5, http://xflr5.sourceforge.net/xflr5.htm, (17-10-2011).

[10] G. H. Bryan, *Stability in Aviation*.: Macmillan and Co., limited, 1911.

[11] Handling Qualities Rating Scale, http://history.nasa.gov/SP-3300/fig66.htm, (17-10-2011).

[12] P. Eden, *The Encyclopedia of Modern Military Aircraft*. London: Amber Books, 2004.

[13] R. H. Bishop, *Modern Control Systems Analysis & Design Using Matlab & Simulink*. United States of America: Addison Wesley Longman, Inc., 1997.

[14] Lawrence Sperry: Autopilot Inventor and Aviation Innovator, http://www.historynet.com/lawrence-sperry-autopilot-inventor-and-aviation-innovator.htm, (17-10-2011).

[15] K.H. Ang, G.C.Y. Chong, and Y. Li, "PID control system analysis, design, and technology," *IEEE Transactions on Control Systems Technology*, vol. 13, no. 4, 2005, pp. 559-576.

[16] J. Luo and L. C. Edward, "Determination of Weighting Matrices of a Linear Quadratic Regulator," *Journal of Guidance, Control and Dynamics*, vol. 18, no. 6, 1995, pp. 1462-1463.

[17] K. Bousson, Y. Elkrief, and D. Bar-Shalom, "Nonlinear Optimal Torque Control of PMSM Systems with Application to Minimum Fuel Attitude Stabilization," *International Review*

of Electrical Engineering, vol. 6, no. 6, 2011, (to appear).

[18] Variable Geometry Wing, http://en.wikipedia.org/wiki/Wing_configuration, (17-10-2011).

[19] The Makhonine 'Telescoping wing', http://www.ww2aircraft.net/forum/other-mechanical-systems-tech/makhonine-telescoping-wing-8527.html, (17-10-2011).

[20] Akaflieg Stuttgart Teleskop-Flügel, http://www.uni-stuttgart.de/akaflieg/index.php?id=49&L=2, (17-10-2011).

[21] Gevers Aircraft, Inc. - Genesis, http://www.geversaircraft.com/home.htm, (17-10-2011).

[22] D. A. Neal et al., "Design and Wind-Tunnel Analysis of a Fully Adaptive Aircraft Configuration," 2004.

[23] P. Gamboa, J. Mestrinho, and J. Felício, "Design Optimization of a Variable-Span Morphing Wing," in *52nd AIAA/ASME/ASCE/AHS/ASC Structures, Structural Dynamics and Materials Conference*, Lisbon, Portugal, 4 - 7 April 2011, Denver, Colorado, pp. Paper no. AIAA 2011-2025.

[24] J. Felício, P. Santos, P. Gamboa, and M. Silvestre, "Evaluation of a Variable-Span Morphing Wing for a Small UAV," in *52nd AIAA/ASME/ASCE/AHS/ASC Structures, Structural Dynamics and Materials Conference*, 4 - 7 April 2011, Denver, Colorado, pp. Paper no. AIAA 2011-2074.

[25] Projecto UAV01 Parte II, http://webx.ubi.pt/~pgamboa/pessoal/2033/2001-2002/Projecto_UAV01_Parte_II.pdf, (17-10-2011).

[26] MATLAB, http://www.mathworks.com/products/matlab/, (17-10-2011).

Appendix

A - UAV “Olharapo” drawings

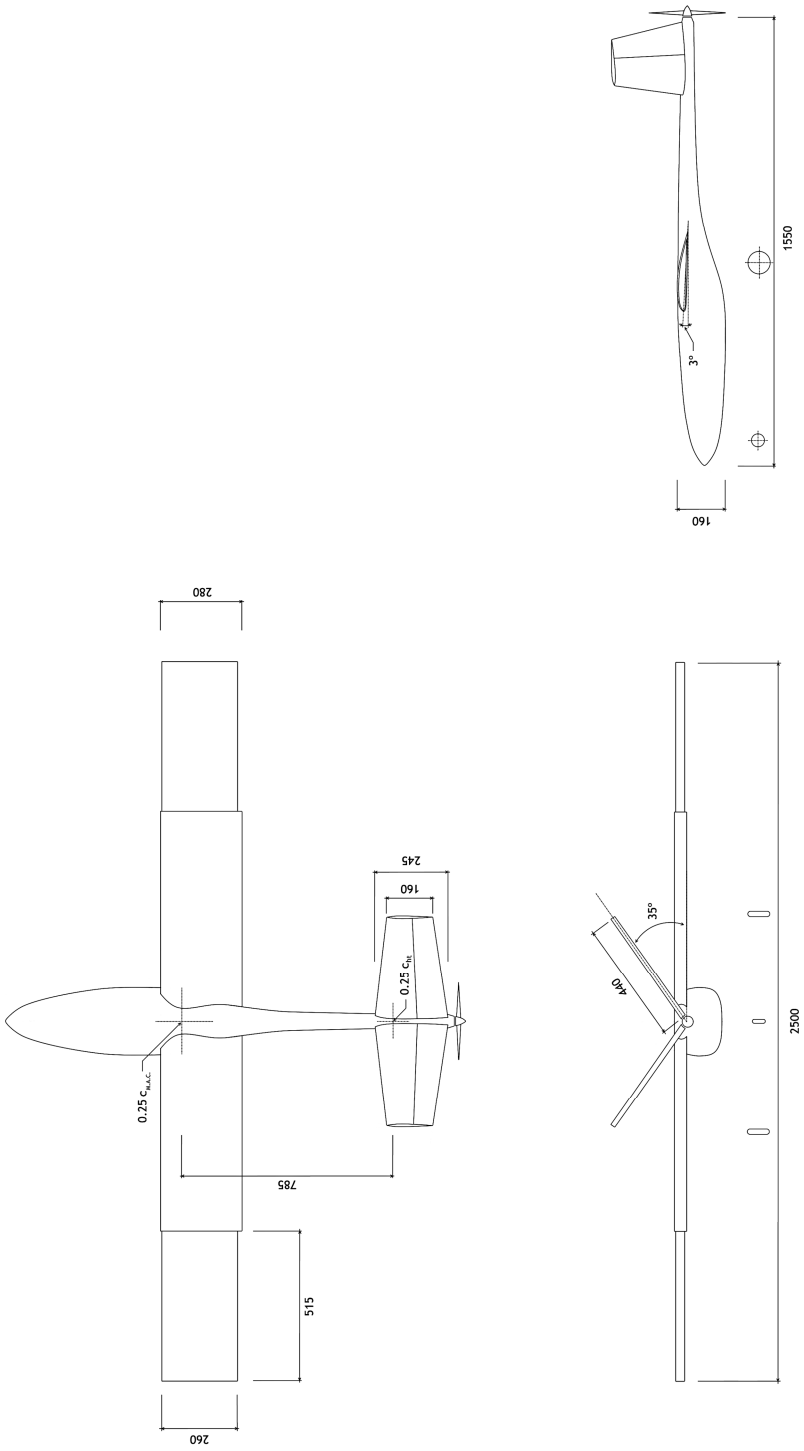

Figure A UAV “Olharapo” drawings

B - Handling Qualities Data

Table A Flight Levels [4]

Level 1	The flying qualities are completely adequate for the particular flight phase being considered.
Level 2	The flying qualities are adequate for the particular phase being considered, but there is either some loss in the effectiveness of the mission, or there is a corresponding increase in the workload imposed upon the pilot to achieve the mission, or both.
Level 3	The flying qualities are such that the aircraft can be controlled, but either the effectiveness of the mission is gravely impaired, or the total workload imposed upon the pilot to accomplish the mission is so great that it approaches the limit of his capacity.

Table B Airplane Classes [4]

Class I	Small, light aircraft (max. weight = 5 000 kg).
Class II	Aircraft of medium weight and moderate manoeuvrability (weight between 5 000 and 30 000 kg).
Class III	Large, heavy aircraft with moderate manoeuvrability (30 000+ kg).
Class IV	Aircraft with high manoeuvrability.

Table C Flight Categories [4]

Non-terminal phase of flight	
Category A	Includes all the non-terminal phases of flight such as those involving rapid manoeuvring, precision tracking, or precise control of the flight path. Included in phase A would be such flight phases as: air-to-air combat (CO), ground attack (GA), weapon delivery (WD), reconnaissance (RC), air-to-air refueling in which the aircraft acts as the receiver (RR), terrain following (TF), maritime search and rescue (MS), close formation flying (FF), and aerobatics (AB).
Category B	Involves the non-terminal phases of flight usually accomplished by gradual manoeuvres which do not require precise tracking. Accurate flight path control may be needed, however. Included in the phase would be: climbing (CL) , cruising (CR) , loitering (LO), descending (D) , aerial delivery (AD) and air-to-air refueling in which the aircraft acts as a tanker (RT).
Terminal phase of flight	
Category C	Involves terminal flight phases, usually accomplished by gradual manoeuvres, but requiring accurate flight path control. This phase would include: take-off (TO), landing (L), overshoot (0s) and powered approach (including instrument approach) (PA).

Tables D and E Longitudinal Phugoid and Short Period flight qualities parameters [4]

Phugoid	Level 1	$\zeta > 0.04$
	Level 2	$\zeta > 0$
	Level 3	T2 > 55s

		Cat. A and C		Cat. B	
		ζ mín	ζ máx	ζ mín	ζ máx
Short Period	Level 1	0.35	1.30	0.3	2.0
	Level 2	0.25	2.00	0.2	2.0
	Level 3	0.15	-	0.15	-

Table F Spiral flight quality parameters [4]

Spiral				
Class	Category	Level 1	Level 2	Level 3
I and IV	A	12 s	12 s	4 s
	B e C	20 s	12s	4 s
II and III	All	20 s	12 s	4 s

Table G Roll flight quality parameters [4]

Roll				
Class	Category	Level 1	Level 2	Level 3
I, IV	A	1.0 s	1.4 s	10 s
II, III	A	1.4 s	3.0 s	10 s
All	B	1.4 s	3.0 s	10 s
I, IV	C	1.0 s	1.4 s	10 s
II, III	C	1.4 s	3.0 s	10 s

Table H Dutch roll flight quality parameters [4]

Dutch roll					
Level	Category	Class	ξ min	$\xi \cdot \omega_n$ min [rad/s]	ω_n min [rad/s]
1	A	I, IV	0.19	0.35	1.0
		II, III	0.19	0.35	0.4
	B	All	0.08	0.15	0.4
	C	I, IV	0.08	0.15	1.0
		II, III	0.08	0.15	0.4

2	All	All	0.02	0.05	0.4
3	All	All	0.02	-	0.4

C - Paper

Roll Motion Control of a Dissymmetrical Wingspan Aircraft

KOUAMANA BOUSSON, FILIPE TAVARES
Dep. of Aerospace Sciences
University of Beira Interior
Convento de Sto. António 6201-001 Covilhã
PORTUGAL
k1bousson@yahoo.com, ftavares87@gmail.com

Abstract: - The present study focuses on the design of a controller for an unmanned aircraft using a variable-span dissymmetric system. This is primarily intended to stabilize roll, although it was designed as a robust system for total control. The system in use is new in its application, being studied similar aircraft built to date. The aircraft for which the system has been designed is an experimental UAV built entirely at the University of Beira Interior. The stability derivatives and other data were obtained with the help of XFLR software. The development and simulation were done using MATLAB, where were tested two different control methods, LQR and Batz-Kleinman controller. A review of the flight dynamics equations for a standard aircraft was originally done, being then adapted this new concept. The interaction between the control surfaces and the response of a general aircraft was studied. An implementation of predetermined flying qualities in order to scale the state weight matrix in the LQR controller for optimal levels was also performed. At the end three separate simulations were performed to confirm the validity of the theoretical system in control and stabilization, for leveled flight when suffering disturbances, and for various equilibrium states described by a sinusoidal equation and a random variation.

Key-Words: - Dissymmetric wing, variable span, UAV, robust controller, roll control, LQR, Batz-Kleinman controller

1 Introduction

Nowadays people tend to look at the sky and see a passing airplane and do not consider the work that is behind it. Building and flying an airplane can be achieved by almost anyone with a basic knowledge of the dynamics of flight, but most simply may not foresee the consequences of a badly designed rudder or a very small dihedral on the main wings. All these mistakes lay on the concepts of stability and control, i.e., a stable airplane is often very easy to control. The optimization of most aspects surrounding an aircraft dynamics requires some mean calculations, and is subject to the various conditions during a flight, i.e., take-off, climbing turn, leveled cruise, approach, landing. For each optimal adjustment of the aircraft control surfaces, span and wing aspect would be preferred as it minimizes the energy losses during flight. Fortunately today airplane enthusiasts are developing a long observed but not easy to build concept: *morphing*. By altering the shape of the wing, for example, the drag forces can be minimized, which allows for a faster flight with the same energy loss. Birds have been doing it since they started flying, and the first men who flew did it without really understanding the benefits it would bring.

The work presented here is organized as follows: in section 2 the problem is described; in section 3 the theory behind the controller design is presented as the problem solution; in section 4 several applications of the two control methods are analyzed and observed; in section 5 conclusions are made on the previous analysis.

2 Problem Statement

The main goal of this system is to fully control the lateral-directional flight variables of the UAV "Olharapo" [1], projected and built at *University of Beira Interior,* with the implementation of a dissymmetric variable-span concept wing. As such, left and right wings are fully automated, and allow the control of the rolling moment by creating an asymmetry in lift distribution. With this, in theory, we can substitute the *aileron* concept completely, but to become a valid control system, it must allow better or at least the same maneuverability as ailerons do. Drag reduction in roll for a dissymmetrical span wing, when comparing it to *ailerons*, is one big advantage [2]. Two different control methods are designed to stabilize every state and control variable to the predefined flight condition, i.e. equilibrium state. The deflection variable for dissymmetric span variation, which substitutes aileron deflection, is now referred as δ_y, where a new approach must be implemented [3].

3 Solution Proposal

An analysis made around the forces acting on an aircraft in-flight leads to the general flight equations that govern its motion. These are composed by small incremental variations of the dimensionless coefficients [4] (stability derivatives) multiplied by the corresponding variables, which depend on the aircraft and flight conditions. The stability derivatives describe the change to a force or moment in response to a variation of a flight variable. In order to fully and precisely determine the influences of the various angles and rates to the moment and force coefficients, it becomes favorable to analyze the airplane in-flight. As this is not viable in project phase, these have to be estimated using several equations available throughout several books [5] [6] [7]. This estimation is based on known flight equations and relations between variables and moments. For this work it is only necessary to analyze the lateral-directional flight behavior and acting forces in flight.

3.1 Lateral-directional Flight Dynamics

For directional flight we consider only the lateral velocity (v), the yaw angle (ψ) and the yaw rate (r); for lateral flight only the bank angle (ϕ) and the roll rate (p). Both movements are interlinked. This is noticed when an airplane makes a controlled turn which induces roll and yaw variations simultaneously.

The sideslip angle is related to the airplane's velocities from [5] [8]:

$$\beta = \operatorname{asin}\frac{v}{V} \tag{1}$$

In the special case when the airplane's velocity (V) matches the same direction as the flight path, i.e., approaching with a lateral wind at constant and relative speed, the yaw angle (ψ) can be related to the sideslip angle (β) by:

$$\psi = -\beta \tag{2}$$

This angle (ψ) is also seen as the bearing of the airplane. As it is an angle which does not depend on any aerodynamic forces or moments (usually associated to the sideslip angle (β) correction), it normally is not considered in the flight equations and does not enter on control purposes [5] [8].

Analyzing now the movement around the vertical plane, we have the bank angle (ϕ), which is obtained from the pressure gradient between the left and right wings, due to a symmetric deflection of the ailerons (δ_a). This symmetric deflection changes the roll moment around the longitudinal axis (C_l) as shown in Fig. 1.

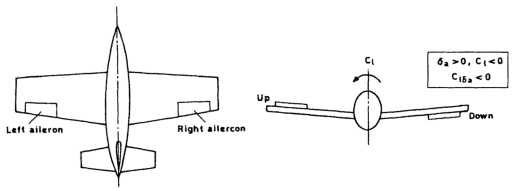

Fig. 1 Aileron deflection and signal convention [5]

With this angle of bank, the aircraft tends to develop a sideslip as shown in Fig. 2, which can be corrected with a deflection of the rudder (δ_r). This way it is comprehensive the need for a linked operation between the ailerons and rudder

control surfaces, in order to perform a leveled turn.

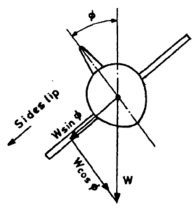

Fig. 2 Development of sideslip due to bank [5]

For this flight mode, similarly to the previous movement, the only applied moment coefficients are [8]:

$$C_D = C_{D_0} + K_{C_D} C_L^2 \quad (3)$$

$$C_y = C_{y_\beta}\beta + C_{y_{\delta_a}}\delta_a + C_{y_{\delta_r}}\delta_r \quad (4)$$

$$C_l = C_{l_\beta}\beta + \frac{b}{2V}\left(C_{l_p}p + C_{l_r}r\right) + C_{l_{\delta_a}}\delta_a + C_{l_{\delta_r}}\delta_r \quad (5)$$

$$C_n = C_{n_\beta}\beta + \frac{b}{2V}\left(C_{n_p}p + C_{n_r}r\right) + C_{n_{\delta_a}}\delta_a + C_{n_{\delta_r}}\delta_r \quad (6)$$

The pitch angle (θ) and therefore the angle of attack (α) are considered null, and the general flight equations are then reduced to [8]:

$$\dot{v} = -\frac{QS}{m}\left(C_D\sin\beta - C_y\cos\beta\right) + g\cos\theta_0\sin\phi - ru_0 + pw_0 \quad (7)$$

$$\dot{p} = \frac{1}{I_xI_y - I_{xz}^2}\left(I_z\left(QSbC_l + \left(I_y - I_z\right)qr\right) + I_{xz}\left(QSbC_n + \left(I_x - I_y + I_z\right)pq - I_{xz}qr\right)\right) \quad (8)$$

$$\dot{r} = \frac{1}{I_xI_y - I_{xz}^2}\left(I_x\left(QSbC_n + \left(I_x - I_y\right)pq\right) + I_{xz}\left(QSbC_l + \left(I_y - I_x - I_z\right)qr - I_{xz}pq\right)\right) \quad (9)$$

$$\dot{\phi} = p + r\cos\phi\tan\theta_0 \quad (10)$$

3.2 Handling Qualities

A trimmed airplane performs a natural frequency motion when disturbed from equilibrium. An airplane is in equilibrium when the resultant forces and moments about the $C.G.$ are equal to zero, and the tendency for an airplane to return to this equilibrium, after a disturbance, is the concept of static stability. For this to happen, the airplane must have restoring moments or forces. In dynamic stability we focus on what happens to the motion of the airplane, when suffering a disturbance, through time. Here we can have two options: oscillatory (damped or undamped) and non-oscillatory motions [9] [7]. The oscillatory modes can be described by a second-order equation, based on the principle of a rigid body coupled to a spring and a damping device [7]. The spring has a natural frequency of ω_n and the damping device a damping ratio of ξ. As such, this system has a characteristic equation in the following form:

$$\lambda^2 + 2\xi\omega_n\lambda + {\omega_n}^2 = 0 \quad (11)$$

Where the two roots, in the form $\lambda = a \pm bi$, are given by:

$$\lambda_{1,2} = -\xi\omega_n \pm i\omega_n\sqrt{1-\xi^2} \quad (12)$$

In lateral flight three modes of motion are present: spiral, roll and Dutch roll (being the last the only oscillatory). Each mode's respective Eigen value is obtained from the characteristic equation of the state matrix A. The spiral movement is the tendency to increase or reduce the wing bank angle after a lateral disturbance [8]. As it is not an oscillatory mode, the corresponding eigenvalue is obtained from a logarithmic function, and the only limiting data is the minimum time to double its amplitude, given by:

$$T_2 = \frac{\log(2)}{-\lambda} \quad (13)$$

The Dutch roll movement resembles a "falling leaf" type oscillation which consists of a combination of yaw and roll motion. The conjugated eigenvalue is determined from eq. (12).

The roll mode, as the spiral mode, is not oscillatory and depends on the bank angle. The only variable that characterizes this eigenvalue is the total roll time and is calculated with:

$$T_t = \frac{1}{-\lambda} \quad (14)$$

3.2.1 Imposed Flying Qualities

To apply custom eigenvalues in control, thus improving the flight characteristics of the aircraft, the theory developed by *Jia Luo and C. Edward Lan* [10] was followed and these are inputted in the vector λ for Q matrix estimation. As such, by inverting the determination of the flying qualities to predetermined data, which was set as Level 1, Class I, Cat. B airplane (Cat. B because it is most adequate for the type of vehicle and missions, the corresponding optimal values to apply in vector λ were then found easily. This predetermined data is found along various books [9] [8] [7]. To accomplish this, the frequency and damping equations were solved in order to the real and imaginary parts of each value. For each movement theory, the corresponding values for a Level 1, Class I, Cat. B airplane are all resumed in Table 1:

Table 1 Level 1, Class I, Cat. B corresponding parameters for each flight mode

	ω_n	ξ	$\xi \cdot \omega_n$	T_2	T_t
Spiral	–	–	–	> 20 s	–
Dutch roll	> 0.4	> 0.08	> 0.15	–	–
Roll	–	–	–	–	< 1.4 s

For the oscillatory mode (Dutch roll), where the complex form $\lambda = a \pm bi$ is used, the following real and imaginary parts of the eigenvalues were determined from equations (15) and (16):

$$a = -\xi \cdot \omega_n \tag{15}$$

$$b = \omega_n \sqrt{1 - \xi^2} \tag{16}$$

The eigenvalues for the two non-oscillatory modes (spiral and roll) need to be obtained from equations (13) and (14), simply solving in order to the Eigen value from equations (17) and (18), respectively:

$$\lambda_s = -\frac{\log(2)}{T_2} \tag{17}$$

$$\lambda_r = -\frac{1}{T_t} \tag{18}$$

Replacing the variables with values from Table 1, it is possible to obtain the optimal Level 1, Class I, Cat. B eigenvalues that are imposed in control, allowing an also optimal Q matrix. The values used are present in Table 2 below:

Table 2 Variables chosen for Eigen value calculation

	ω_n	ξ	$\xi \cdot \omega_n$	T_2	T_t
Spiral	–	–	–	23 s	–
Dutch roll	0.60	0.70	0.42	–	–
Roll	–	–	–	–	0.10 s

The final vector composed of all these calculated eigenvalues (eigenvector) which is used in control is given by (19):

$$\lambda = [\lambda_r \quad \lambda_{dr\,1,2} \quad \lambda_s] = \lambda = [-10.0 \quad -0.42 \pm 0.4285i \quad -0.0301] \tag{19}$$

3.3 Control with Classical Surfaces

Up to now we have seen how is the dynamics of an airplane influenced by the deflection of control surfaces and a disturbance of the flight conditions. In case of a small disturbance of the equilibrium flight conditions we define, most airplanes are not sufficiently stable to return to this previous state [5]. Nowadays systems have evolved and an automatic controller can effectively maintain the attitude of an airplane by means of an actuator and electrical motor (Fig. 3) enabling the pilot to concentrate more on other aspects of flight. The amount of energy required to operate a poorly designed airplane is also a negative factor, and minimizing this energy loss is the main characteristic of an optimal control system.

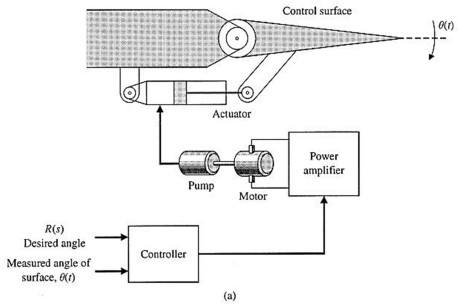

Fig. 3 Control system scheme [11]

When designing a complete state regulator for an airplane, the full system block diagram becomes crucial to understand and to further build it physically. This scheme is composed by all the sub-systems that influence the flight variables, either being motion sensors or

controlling elements. Generally, an AFCS (*Automatic Flight Control System*) is represented as shown in Fig. 4. For specific motion regulators (i.e., lateral motion, specific state variables) a simplified system is designed but based on the same general idea.

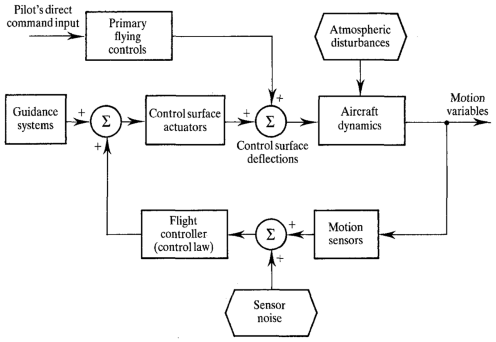

Fig. 4 General block diagram of an AFCS [9]

Nowadays there are several methods [8] [12] to stabilize the attitude variables of an aircraft. The most commonly used is the PID controller (proportional–integral–derivative controller) [13], which calculates an error value as the difference between a measured process variable and a desired objective point, and then attempts to minimize this error by adjusting the process control inputs. A better alternative to this method is the use of a LQR controller.

3.3.1 LQR Controller

LQR stands for *Linear Quadratic Regulator*. Implementing a LQR controller implies operating a dynamic system at minimum cost with supplied weight factors (R and Q matrices). This system dynamics must be described by a set of linear differential equations, which, in the case of the non-linear flight equations from equations (7) to (10), these need to be linearized. As such, a continuous-time linear system is described by [14] [5] [9] [8] [6]:

$$\begin{cases} \dot{x} = Ax + Bu \\ y = Cx + Du \end{cases} \tag{20}$$

The cost function is defined as:

$$J = \int_0^{\infty} F(x,u)\,dt \tag{21}$$

Where:

$$F(x,u) = x^T Q x + u^T R u \tag{22}$$

Q and R are weighting matrixes for state and control variables, respectively, and must be positive-definite (being Q positive semi-definite). The feedback control law that minimizes the cost equation in (21) is:

$$u = -Kx \tag{23}$$

K is the system's gain matrix with m lines and n columns ($K \in \mathbb{R}^{m\,x\,n}$) and is determined by:

$$K = R^{-1}B^T P \tag{24}$$

P is found by solving the continuous time algebraic Riccati [8] equation:

$$A^T P + PA - PBR^{-1}B^T P + Q = 0 \tag{25}$$

The main problem with properly (optimally) scaling a LQR controller is finding the adequate weighting factors R and Q, and this somehow limits the utilization of this controller. R and Q can be simply determined using *Bryson's* method [8], where each state and control weight is calculated in relation to its maximum amplitude:

$$Q_{ii} = {}^{1}\!/_{x_{i,max}^2} \qquad R_{ii} = {}^{1}\!/_{u_{i,max}^2} \tag{26}$$

Jia Luo and C. Edward Lan [10] purposed one other method for this estimation. The R matrix is still determined as in (26) and the problem lies in the determination of an optimal Q. For this it is necessary to first minimize the cost function J (21) by use of the *Hamiltonian* matrix (H) which is used to determine (P) in LQR. This matrix (H) is defined as:

$$H \in \mathbb{R}^{2n\times 2n} \equiv \begin{bmatrix} A & -BR^{-1}B^T \\ -Q & -A^T \end{bmatrix} \tag{27}$$

The eigenvalues of this matrix are symmetrically distributed along the imaginary axis, thus having positive and

negative symmetric real parts. To determine those eigenvalues, the following algebraic equation needs to be solved:

$$\det(\lambda_i I - H) = 0 \quad (28)$$

With this equation (28) we can also determine the matrix Q, but for this the eigenvalues (λ_i) need to be assumed, which gives us some power for optimization. For simple calculations it is enough to use the eigenvalues of the state matrix A, but if we want to minimize the cost function J (21) imposing certain flight qualities, these eigenvalues are then subject to our needs. The weighting matrix Q is defined by one single diagonal composed with a vector $q_i = (q_1, q_2, \dots, q_n)$. The problem is finding the q_i that satisfies eq. (28), and one can do that by minimizing the following equation system:

$$f_i(q_i) = \det(\lambda_i I - H(q_i)) = 0 \quad (29)$$

Being:

$$Q_{ii} = q_i \quad (30)$$

As Q is positive semi-definite, in case of any of the diagonal values found with solving (29) being negative, we can simply elevate them to square. Another way is to use the absolute value of any negative element. This enables us to find the right R and Q. The control law to apply in the controller as the feedback system is given by (23). The system stabilizes around zero with this equation.

3.3.2 Batz-Klienman Controller

This method is very similar to the LQR method, except the gain matrix K (24) is here seen as an L matrix, as it is defined by [12]:

$$L = B^T * P(\tau)^T \quad (31)$$

Where P is now defined by the *Gramian* as [12]:

$$P(\tau) = \int_0^\tau e^{-A*t} * B * B^T * e^{-A^T*t} dt \quad (32)$$

A variable τ appears here to limit the integration interval and is assumed (always positive) for optimization purposes. The smaller the variable τ, the smaller the control amplitude, and the faster it converges for optimal values. The control law here is the same as LQR but with the L matrix defined in (31):

$$u = u_{ref} - L(x - x_{ref}) \quad (33)$$

3.4 Dissymmetrical Span Control

The dissymmetrical wing system consists of two fully retractable and autonomous wing sections, each moved by a servo and rack mechanism. In Fig. 5 the final mechanical system can be observed. All design and construction was developed over the last two years by two other aeronautic students.

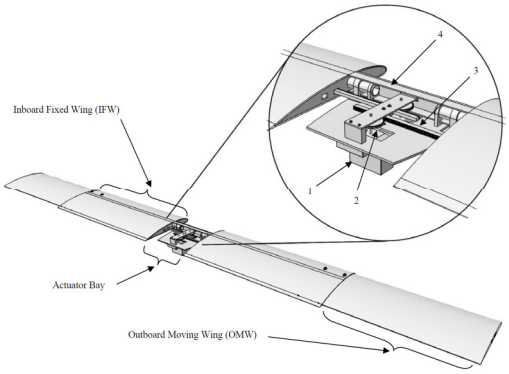

Fig. 5 Variable-Span Wing mechanical system (1-servo-motor; 2- transmission pinion; 3-transmission rack; 4-carbon spar) [15]

The system must provide roll authority equivalent to the authority provided by the use of ailerons, which means that, for one of the wings, the variation in roll moment coefficient with the deflection of the control surface (or flap) is given by [8] [7]:

$$C_{l_{\delta_a}} = \frac{dC_l}{d\delta_a} = \frac{2C_{l_\alpha}\tau}{Sb}\int_{y_1}^{y_2} cy\, dy \quad (34)$$

Where, τ here refers to the flap effectiveness parameter [7], and y_1, y_2 are the limits of the control surface as in Fig. 6.

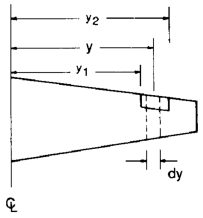

Fig. 6 Theory for aileron effectiveness approximation [7]

Gamboa et al. [3] demonstrated that, for a symmetric variable span morphing wing and assuming the wing's lift distribution to be perfectly elliptical, moving the elliptic center along the y-axis, it is possible to obtain $C_{l_{\delta_y}}$ the following way:

$$C_{l_{\delta_y}} = \frac{8W}{\pi b \rho V^2 S_{ref} b_{ref}} \int_{-b'}^{b''} y \sqrt{1 - \left(\frac{2(y - y')}{b}\right)^2}\, dy \quad (35)$$

Where, b' and b'' refer to the left and right span dimensions, respectively; y is the length of a semi-wing, and y' is the span deflection. b_{ref} is the wing's maximum span which differs from $b = b' + b''$. One other derivative takes a direct part in roll motion and was analyzed in this work as well. The damping-in-roll, or C_{l_p}, is the influence of the roll rate p on the roll moment coefficient C_l, also seen as the tendency for an airplane to roll. From the same analysis made for estimating $C_{l_{\delta_y}}$, the damping-in-roll derivative can be estimated as:

$$C_{l_p} = -\frac{1}{V S_{ref} b_{ref}} \int_{-b'}^{b''} a_{0_y}(y) \sqrt{1 - \left(\frac{2(y - y')}{b}\right)^2}\, c(y) y^2 dy \quad (36)$$

The roll, yaw and lateral force coefficient equations where the new derivatives take part were modified by simple substitution. This was studied as the equations are composed by incrementing each influential dynamic variable multiplied by its derivative. As such, and with the help of XFLR5 v6.03 software [16], the work was simplified a lot. The analysis is then made according to the resultant differential lift (ΔL) below (37) [7]:

$$\Delta C_l = \frac{\Delta L}{Q S_{ref} b_{ref}} = \frac{C_L c(y) dy}{S_{ref} b_{ref}} \quad (37)$$

By obtaining the lift coefficient (C_L) distribution from XFLR, iterating for various positions of the deflected wing, the resulting variation of the roll moment coefficient (C_l) due to a deflection of the right wing, and symmetrically for the left side, can be seen in Fig. 7:

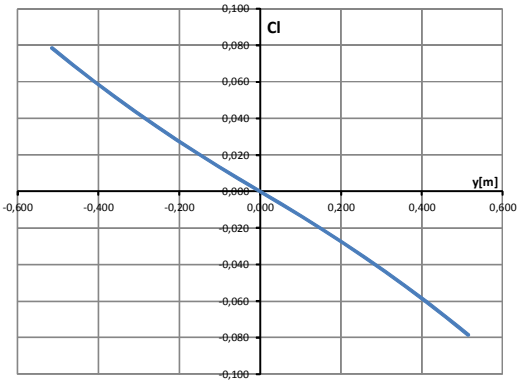

Fig. 7 Roll moment coefficient (C_l) distribution due to wing deflection (y)

A positive deflection of a wing results in a negative variation of roll moment, as the lift increases on the deflected side. The influence in yaw moment by *aileron* deflection can be ignored as the control surfaces are reversely linked, i.e., the increase in drag is assumed equal for the left and right *ailerons*. For design and control purposes this means an inconsideration of adverse yaw [7]. As the variable span system works by deflecting only one wing at a time, the variation of drag is not symmetric, and as such, must be considered. A positive deflection (see Fig. 9) of one wing span implies a positive yaw moment increase. To determine an approximate yaw moment variation due to the variation in span, a similar approach as to roll moment (Fig. 7) was made taking in consideration the total drag coefficient distribution from XFLR analysis, influenced by the parasite and induced drag coefficients ($C_{D,0}, C_{D,i}$). The resulting yaw moment variation was estimated by equation (38), and represented in Fig. 8:

$$\Delta C_n = \frac{\Delta D}{QS_{ref}b_{ref}} = \frac{(C_{D,0} + C_{D,i})c(y)dy}{S_{ref}b_{ref}} \quad (38)$$

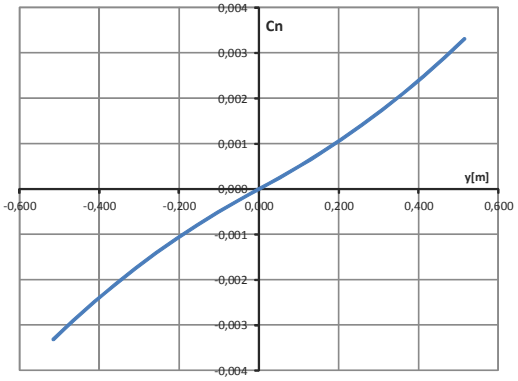

Fig. 8 Yaw moment coefficient (C_n) distribution due to wing deflection (y)

From the two distributions in Fig. 7 and Fig. 8, the control derivatives for $C_{l\delta y}$ and $C_{n\delta y}$ can be obtained. The results are present in Table 4 below. The remaining derivative that measures the relation between the wing deflection and the lateral force, $C_{y\delta y}$, can be ignored as laterally it does not influence in a measurable amount. The C_{l_p} and C_{n_r} derivatives, which are affected by induced roll and yaw due to the V-Tail, were assumed from the data obtained in XFLR simulations [6]. All other derivatives were estimated using XFLR. Weight, traction and dimensions were obtained from direct measurements on the airplane. As the UAV is V-Tailed, the respective deflection components for elevator and rudder are replaced as δ_{V_e} and δ_{V_r}, respectively. Other derivatives which refer to these control variables are accordingly written as well.

Running the simulation for a zero angle of attack, the following coefficients were obtained:

Table 3 Zero angle of attack coefficients

C_{L0} = 0.19664	C_{D0} = 0.01652	C_{m0} = 0.03526

The final stability and control derivatives for lateral-directional flight are:

Table 4 Lateral-directional stability and control derivatives

$C_{y\beta}$ = -0.17991	$C_{l\beta}$ = -0.04508	$C_{n\beta}$ = 0.05733	C_{lp} = -0.55989
C_{np} = -0.05572	C_{lr} = 0.14868	C_{nr} = -0.03924	$C_{l\delta y}$ = 0.1467
$C_{n\delta y}$ = -0.006	$C_{y\delta Vr}$ = 0.040083	$C_{l\delta Vr}$ = -0.054716	$C_{n\delta Vr}$ = -0.021383

The following derivatives were assumed null as only a very small influence is expected from those:

$$C_{L\dot{\alpha}}, C_{m\dot{\alpha}}, C_{y\delta y} = 0 \quad (39)$$

To control, one main consideration to take is the dimension of the wing deflection. By taking measurements in the already built airplane "Olharapo", it was noticed that the wing span varies between 1470 millimeters for both wings retracted, and 2500 millimeters for both wings fully extended. This means that each movable wing extends about 515 millimeters, and the wing is able to alter its span by almost double. To apply this in the control, some notions had to be developed. The δ_y control variable is limited by -0.515 to +0.515 meters so that it resembles the working method of all other control variables. Flying with both wings extended (or both wings retracted) refers to a null δ_y. With this notion, the wing deflection is related to the actual working scheme as showed in Fig. 9. Note that the controller is dimensioned for a cruise speed of 20 meters per second, which stands about half its projected speed envelope, as seen in Fig. 10:

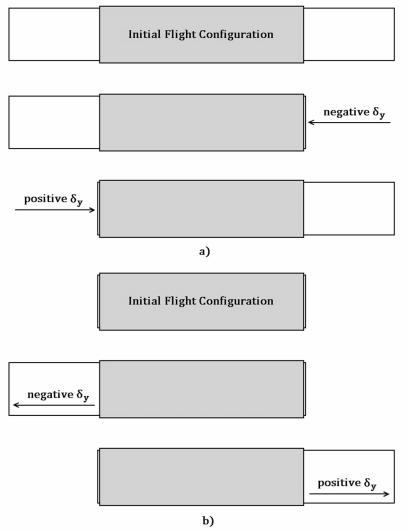

Fig. 9 Wing deflection variable for: a) Flight with wings extended, below 20 m/s; b) Flight with wings retracted, above 20 m/s

As studied by *Gamboa et al.* [3] two years ago, the vehicle's speed efficiency in relation to wing span shows that the best flying condition is wings fully extended. For higher velocities, the most efficient scheme is wings fully retracted. This created a need of two distinct flying modes, as shown in Fig. 9. The code was written considering the airplane is flying leveled with wings fully extended, which refers as Fig. 9 a) for the related wing deflections signals.

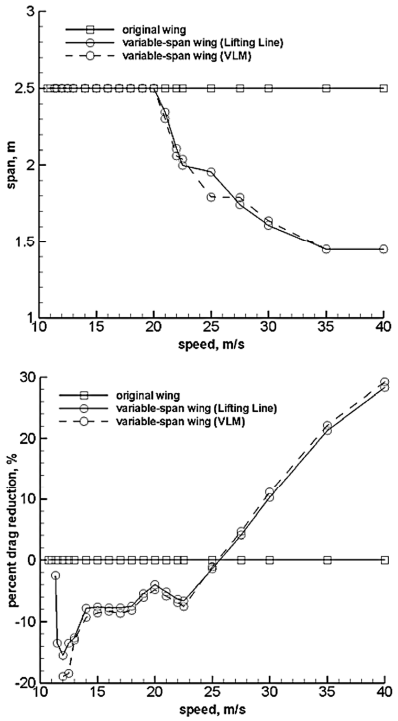

Fig. 10 Span variation with flight speed (left) and drag reduction relative to original wing (right) for the original and variable-span wings [3].

The resulting data constants to be applied in the flight equations are:

Table 5 Aircraft and flight conditions data

Take-off weight: 6.700 kg	Altitude: 0 m (Sea Level)
Span (maximum span): 2.500 m	Flight speed: 20 m/s
Wing median chord: 0.27 m	Engine traction: 25 N (assumed)

With this data we have the necessary conditions to project a controller. These values are subject to change as the UAV is still under development and testing, but the obtained derivatives are already very close to those that would be found with a full *wind-tunnel* or *in flight* analysis.

4 Applications

In order to fully demonstrate and test the validity of a controlled dissymmetrical span system described in this work, the following analysis was made using MATLAB [17] software. Taking full use of the mathematical and programming tools provided, the simulation of a control response after a disturbance or equilibrium change was applied with ease.

4.1 Classical Control Method (Disturbance Response)

The most classic method to analyze is the simulated state variable response for an atmospheric disturbance of the trimmed control surfaces, in order to return all state variables to the previous equilibrium point. As such, to accomplish this, a code was written following the order in Fig. 11, where all parts were already explained in detail along previous chapters.

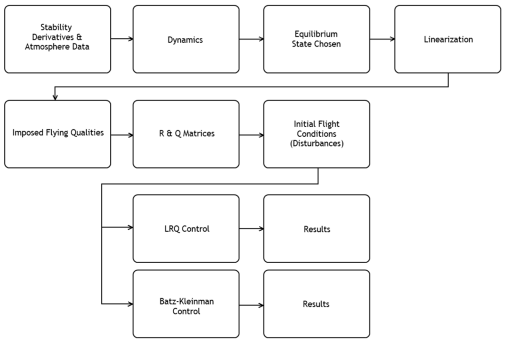

Fig. 11 Diagram of program simulation flow scheme (in general)

The disturbance can be defined by a uniform fractioned divergence from the equilibrium state variables defined before, or by inputted values from the user. The equilibrium is obtained by linearizing the system using, for example, *Taylor's* equation [8]. This simulation is performed at sea level altitude and a cruise speed of 20 m/s, at leveled flight, from Table 5. The equilibrium state and control variables obtained from solving $f(x_{eq}, u_{eq}) = f(x_0, u_0) = 0$, which gives the results found in Table 6 and Table 7.

Table 6 Equilibrium State constants

$u = 20$ m/s	$w = 0$ m/s	$q = 0$ rad/s
$\theta = 0.0481$ rad	$v = 0$ m/s	$p = 0$ rad/s
$r = 0$ rad/s	$\phi = 0$ rad	$\psi = 0$ (not considered)

Table 7 Equilibrium Control constants

$\delta_{V_e} = -0.0180$ rad	$\delta_T = 16.89\%$	$\delta_y = 0$ m	$\delta_{V_r} = 0$ rad

The state and control vectors are then defined as:

$$x = \begin{bmatrix} u \\ w \\ q \\ \theta \\ v \\ p \\ r \\ \phi \end{bmatrix} = \begin{bmatrix} 20 \\ 0 \\ 0 \\ 0.0481 \\ 0 \\ 0 \\ 0 \\ 0 \end{bmatrix}; \; u = \begin{bmatrix} \delta_{V_e} \\ \delta_T \\ \delta_y \\ \delta_{V_r} \end{bmatrix} = \begin{bmatrix} -0.0180 \\ 0.1689 \\ 0 \\ 0 \end{bmatrix} \quad (40)$$

Note that the leveled flight condition is achieved with 17% power and a small positive pitch of about 2.7 deg, which is maintained with a negative elevator (nose up) deflection of about 1 deg. For this work, and so that the aircraft is not excessively perturbed, small disturbances to every state variable were applied. As such, the disturbance vector to apply in the LQR and Batz-Kleinman calculation is:

$$x_d = \begin{bmatrix} 22 \\ -2 \\ -0.03 \\ 0.0181 \\ 2 \\ 0.03 \\ 0.03 \\ 0.03 \end{bmatrix} \quad (41)$$

The objective of this simulation is that the controller fully stabilizes in about 6 seconds. Running the simulated initial conditions and with the imposed Level 1 handling qualities, the UAV is then able to return to its lateral-directional equilibrium state, as observed in Fig. 12 and Fig. 13 below:

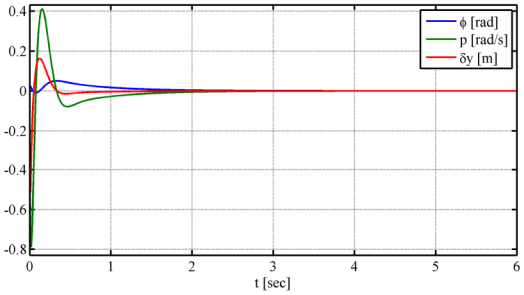

Fig. 12 Bank angle, roll rate, and span deflection for LQR – Classic Simulation

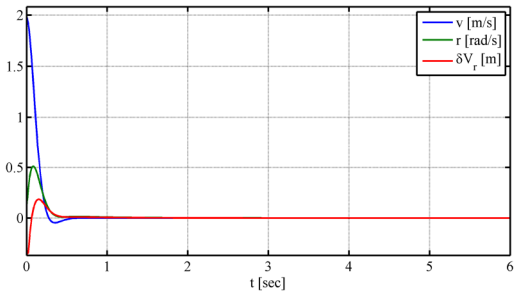

Fig. 13 Lateral velocity, yaw rate, and rudder deflection for LQR – Classic Simulation

For the Batz-Kleinman controller, there is no influence from the imposed eigenvalues, thus this control method differs from the LQR method by a small number of parameters. This controller relies on the calculation of the P matrix from solving the *Gramian* integral in (32). The only optimizing data is the number of intervals for the integral estimation (n), which was set at $n = 400$, and the final integration value τ, set at $\tau = 0.3$. Higher values of τ provide a more oscillating stabilization, as the integral limits start to diverge from the linearized boundaries. The remaining simulation data was the one used for the LQR method, and the UAV stabilizes in a similar way as before as seen in Fig. 14 and Fig. 15:

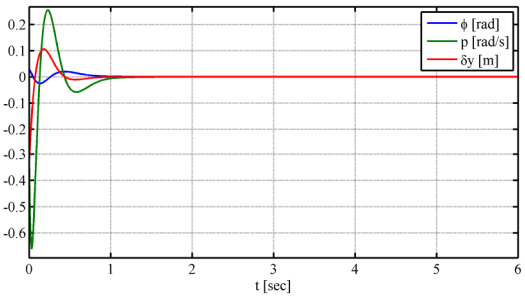

Fig. 14 Bank angle, roll rate, and span deflection for Batz-Kleinman – Classic Simulation

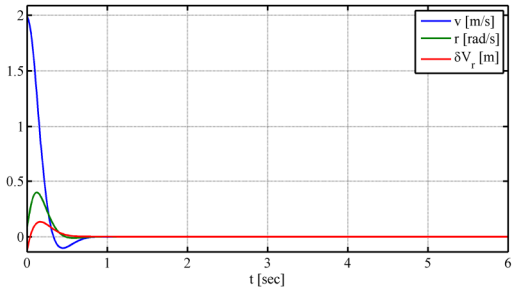

Fig. 15 Lateral velocity, yaw rate, and rudder deflection for Batz-Kleinman – Classic Simulation

As can be seen, both methods stabilize in less than 3 seconds, being Batz-Kleinman's the most efficient (energy wise, and time wise), but also very hard on control actuation for smaller values of τ. As the Q matrix was dimensioned assuming a very responsive and stable airplane (Level 1, Class I, Cat. B) the LQR control data is also very smooth. The simulations were performed for a very small disturbance of the bank angle (as well as other variables) and the dissymmetric variation of the wings for control can be recognized in Fig. 12 and Fig. 14. The wing control system uses about $1/6$ of its maximum deflection for LQR and $1/10$ for Batz-Kleinman's (seen in red).

4.2 Bank Angle Sinusoidal Variation

On the classical simulation the relationship between the induced control and consequent reaction in state variables was not easy to see. As such, a more complex analysis was performed. For this simulation, a large number of equilibrium states were calculated, varying only the bank angle ϕ with a sinusoidal function in order to force the UAV to perform a variable turn to, i. e., avoid an obstacle such as a tree or building. The maximum bank angle was set to 30 degrees. The remaining data used before is also inputted here, and the imposed flight qualities used are the same for each equilibrium state (which is an approximation as the bank angle is reduced). Every fixed number of seconds the UAV changes its bank angle and a new equilibrium point and controller is dimensioned. This way it is possible to see the reactions of state and control variables and proving the concept mechanism works. To induce a full smooth symmetric amplitude in bank, the bank angle ϕ follows the curve in Fig. 16:

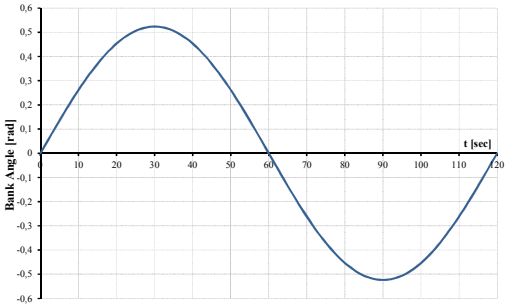

Fig. 16 Sinusoidal variation of the bank angle (maximum bank 30 degrees, time 120 seconds)

This represents the following equation:

$$\phi = \frac{|\phi_{max} - \phi_{min}|}{2} \cos\left[\left(\frac{2\pi}{(t_{max} - t_{min})}\right)\left(t + \frac{3}{4}(t_{max} - t_{min})\right)\right] \quad (42)$$

The total simulation time span is 120 seconds, and a number of 20 equilibrium points were calculated (for 20 bank angle positions). However, the simulation was run for a total time of $\left(120 + \frac{120}{20}\right) = 126$ seconds to enable a return to the initial values, meaning a time of 6 seconds between equilibrium points. Each 6 seconds of simulation the angle varies and forces the controller to move to the next equilibrium point, always considering the previous stable (or nearly stable for the small stabilization time) variables for state and control as the initial values used next. The obtained results follow the bank sinusoidal distribution as can be observed in Fig. 17 and Fig. 18 for the LQR implementation and in Fig. 19 and Fig. 20 for Batz-Kleinman.

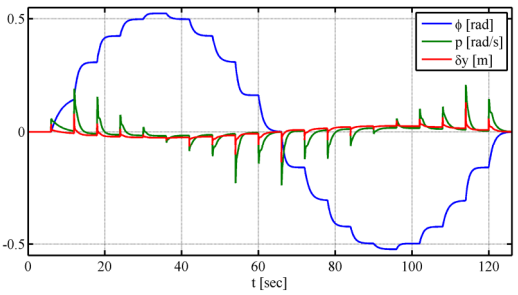

Fig. 17 Bank angle, roll rate, and span deflection for LQR – Sinusoidal Simulation

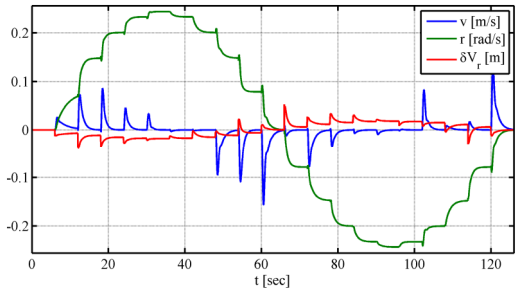

Fig. 18 Lateral velocity, yaw rate, and rudder deflection for LQR – Sinusoidal Simulation

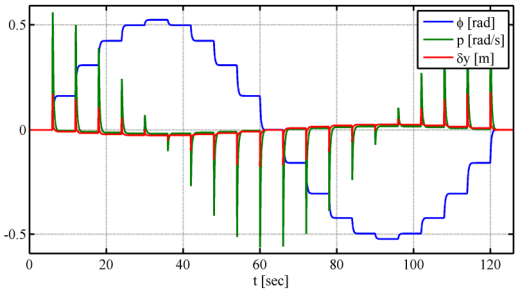

Fig. 19 Bank angle, roll rate, and span deflection for Batz-Kleinman – Sinusoidal Simulation

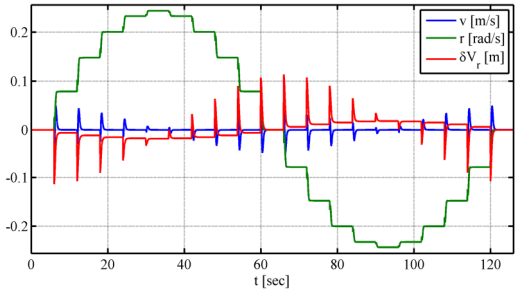

Fig. 20 Lateral velocity, yaw rate, and rudder deflection for Batz-Kleinman – Sinusoidal Simulation

Small differences occur as seen before in smoothness, stabilization time, and energy use, as the Batz-Kleinman is much faster to stabilize than the LQR. In Fig. 17 and Fig. 19 a small deflection of right and then left wings is observed as the curve angle is increased to maintain a maximum bank of 30 degrees in both directions. Previous classic control method results did not evidence the controller response to each change of attitude as can be seen here. Positive and negative responses that indicate the airplane's position in space are now observed fully. As the bank increases, the aircraft is more stressed, and to maintain this flight condition the control variables suffer an increase in variation. The span variation is opposite in signal to the bank angle, which had been acknowledged with the description of the system in Fig. 9. For a bank of 30 degrees the wing deflects no more than a few centimetres. The roll rates (in green) are distributed in a shifted phase related to the bank angle: the smaller the change in bank, the smaller the needed roll rate. For a positive change of bank, a positive rate is observed as would be expected, as for an almost null rate when at maximum bank.

4.3 Random Bank Angle Variation (Two Step Maximum)

For this simulation the last equilibrium states (sinusoidal simulation) were used. The difference lies in the controller simulation, as for this simulation, every 6 seconds the program chooses a random point, no more than two steps above or below the previous equilibrium value. As the same conditions and determined variables were used, the stabilization aspect for each equilibrium state is equal to that seen in the last one. The random variable that determines the next equilibrium was created using only MATLAB's [17] commands, giving two different results, one for each control method.

Running the code with these random values for simulation LQR and Batz-Kleinman's control methods returned the following results present in Fig. 21 to Fig. 24:

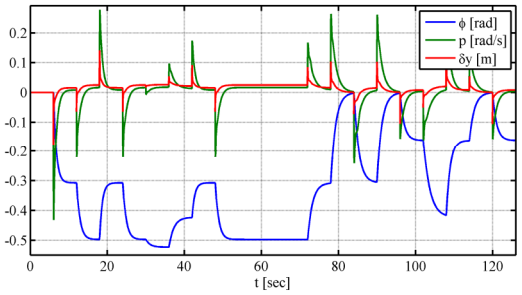

Fig. 21 Bank angle, roll rate, and span deflection for LQR – Random Simulation

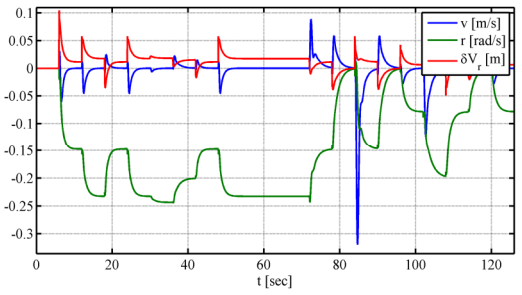

Fig. 22 Lateral velocity, yaw rate, and rudder deflection for LQR – Random Simulation

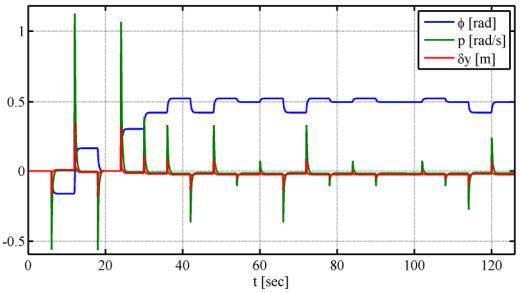

Fig. 23 Bank angle, roll rate, and span deflection for Batz-Kleinman – Random Simulation

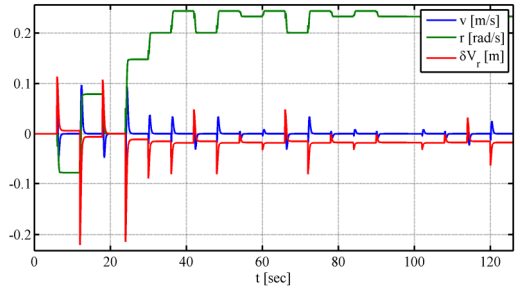

Fig. 24 Lateral velocity, yaw rate, and rudder deflection for Batz-Kleinman – Random Simulation

A random simulation of this kind is representative of a constant change in direction due to the bank variation and respective change of turn. For this analysis, the main aspect is the ability of the airplane to stabilize given an unknown next equilibrium state. The response of wing deflection due to bank is shown in detail in Fig. 21 and Fig. 23, which is similar to previous simulations except to the fact that every 6 seconds an unknown bank is used. Both controller methods are subject to further optimizations, as both allow a "tuning" to comply with required conditions. The LQR is more tolerant to this as there are various aspects than can be optimized but requires much more analysis time to adjust them. The Batz-Kleinman is less open to optimizations, but is the most reliable, control wise.

5 Conclusions

A variable-span dissymmetric morphing wing mechanism allows, as explained over this work, the full replacement of the standard aileron system. The moment created around the longitudinal axis of the airplane is now done by the differential pressure from the change in wing span. The main objective of this system is the reduction of drag with wing deflection for roll and for leveled cruise, when flying with both wings retracted, enabling a longer cruise and faster speed. As it requires a more complex building process and heavier parts, it is a valuable challenge. The implementation of a controller to stabilize the roll motion of the airplane automatically after a disturbance or to follow specified equilibrium points is the main focus of this work, not only to perform roll control, but also to stabilize every other flight variable. This allows a fully operational controller.

Two control methods were tested, LQR and Batz-Kleinman controller. A classic disturbance and controller response proved the good stability convergence to equilibrium values, occurring before five seconds of simulation time. Both methods proved to work equally fine, being the LQR the only optimizing one by tempering with the weights matrices. The Batz-Kleinman method originated the best results with the faster convergence.

Second and third simulations were made to analyze the influence of sequential and random variations of the same bank related equilibrium points used. To these simulations the results show that the airplane responds well to every variation, stabilizing always in less than the differential time used between each change. Again, the best results were achieved with the Batz-Kleinman control method. The LQR method also performed well, but is not as smooth when comparing both controllers. In general the airplane responded very well to every disturbance forced and every change in bank angle, proving this new concept works, in theory. A real system needs to take in account many other negative aspects that worsen the flying motion and control, such as vibrations, lag in servos, interference, and weather conditions at the time.

With my work, only the surface was touched along a tedious implementation of a fully working controlling system. Indeed, further work needs to be developed to allow the physical integration of a real autopilot system on the UAV, as well as thorough testing procedures to ensure that nothing goes wrong in-flight.

References:

[1] Projecto UAV01 Parte II, http://webx.ubi.pt/~pgamboa/pessoal/2033/2001-2002/Projecto_UAV01_Parte_II.pdf, (17-10-2011).

[2] Gevers Aircraft, Inc. - Genesis, http://www.geversaircraft.com/home.htm, (17-10-2011).

[3] P. Gamboa, J. Mestrinho, and J. Felício, "Design Optimization of a Variable-Span Morphing Wing," in *52nd AIAA/ASME/ASCE/AHS/ASC Structures, Structural Dynamics and Materials Conference*, 4 - 7 April 2011, Denver, Colorado, Paper no. AIAA 2011-2025.

[4] B. L. Stevens and F. L. Lewis, *Aircraft Control and Simulation*. United States of America: John Wiley & Sons, Inc., 1992.

[5] B. N. Pamadi, *Performance, Stability, Dynamics and Control of Airplanes*. United States of America: American Institute of Aeronautics and Astronautics, Inc., 1998.

[6] B. Etkin and L. D. Reid, *Dynamics of Flight Stability and Control, 1996.* United States of America: John Wiley & Sons, Inc., 1996.

[7] R. C. Nelson, *Flight Stability and Automation Control*. United States of America: McGraw-Hill, 1989.

[8] B. D. O. Anderson and J. B. Moore, *Linear Optimal Control*.: Prentice-Hall, 1989.

[9] D. McLean, *Automatic Flight Control Systems*. United Kingdom: Prentice-Hall International, 1990.

[10] J. Luo and L. C. Edward, "Determination of Weighting Matrices of a Linear Quadratic Regulator," *Journal of Guidance, Control and Dynamics*, vol. 18, no. 6, 1995, pp. 1462-1463.

[11] R. H. Bishop, *Modern Control Systems Analysis & Design Using Matlab & Simulink*. United States of America: Addison Wesley Longman, Inc., 1997.

[12] K. Bousson, Y. Elkrief, and D. Bar-Shalom, "Nonlinear Optimal Torque Control of PMSM Systems with Application to Minimum Fuel Attitude Stabilization," *International Review of Electrical Engineering*, vol. 6, no. 6, 2011, (to appear).

[13] K.H. Ang, G.C.Y. Chong, and Y. Li, "PID control system analysis, design, and technology," *IEEE Transactions on Control Systems Technology*, vol. 13, no. 4, 2005, pp. 559-576.

[14] M. J. Abzug and E. E. Larrabee, *Airplane Stability and Control*, Second Edition ed. United Kingdom: Cambridge University Press, 2002.

[15] J. Felício, P. Santos, P. Gamboa, and M. Silvestre, "Evaluation of a Variable-Span Morphing Wing for a Small UAV," in *52nd AIAA/ASME/ASCE/AHS/ASC Structures, Structural Dynamics and Materials Conference*, 4 - 7 April 2011, Denver, Colorado, Paper no. AIAA 2011-2074.

[16] XFLR5, http://xflr5.sourceforge.net/xflr5.htm, (17-10-2011).

[17] MATLAB, http://www.mathworks.com/products/matlab/, (17-10-2011).